Cell Reports

Article

Genetics of yellow-orange color variation in a pair of sympatric sulfur butterflies

Graphical abstract

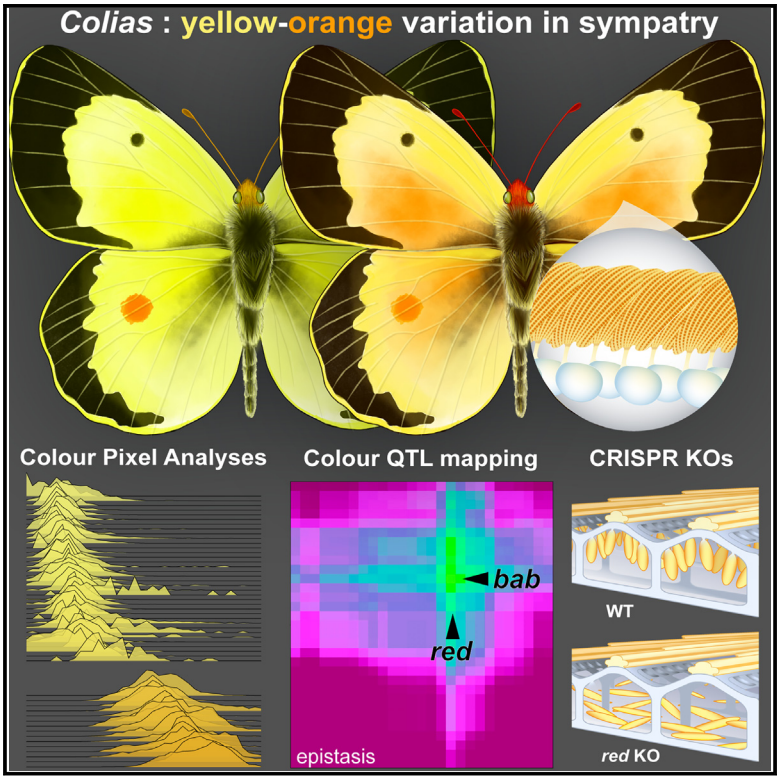

Authors

Joseph J. Hanly, Caroline M. Francescutti, Ling S. Loh, ..., Marshall A. Nakatani, Adam H. Porter, Arnaud Martin

Correspondence

joe.hanly@gmail.com (J.J.H.), aporter@umass.edu (A.H.P.), arnaud@gwu.edu (A.M.)

In brief

Hanly et al. describe a between-species color polymorphism in *Colias* butterflies that displays continuous variation in laboratory crosses. They use QTL analyses and CRISPR-Cas9 mutagenesis to identify candidate genes and find two loci that explain most of the color variation.

Highlights

- Two *Colias* sulfur butterfly species vary in yellow-orange hue
- Color pixel analyses allow precise color quantification
- QTL map shows two major loci explaining most color variation
- CRISPR KOs highlight color-tuning roles of *red* and *bab* QTL candidate genes

Hanly et al., 2023, Cell Reports *42*, 112820
August 29, 2023
https://doi.org/10.1016/j.celrep.2023.112820

CellPress

Cell Reports

CellPress
OPEN ACCESS

Article

Genetics of yellow-orange color variation in a pair of sympatric sulfur butterflies

Joseph J. Hanly,[1,2,4,*] Caroline M. Francescutti,[1] Ling S. Loh,[1] Olaf B.W.H. Corning,[1] Derek J. Long,[1] Marshall A. Nakatani,[1] Adam H. Porter,[3,*] and Arnaud Martin[1,*]

[1]Department of Biological Sciences, The George Washington University, Washington, DC, USA
[2]Smithsonian Tropical Research Institute, Gamboa, Panama
[3]Department of Biology, University of Massachusetts Amherst, Amherst, MA, USA
[4]Lead contact
*Correspondence: joe.hanly@gmail.com (J.J.H.), aporter@umass.edu (A.H.P.), arnaud@gwu.edu (A.M.)
https://doi.org/10.1016/j.celrep.2023.112820

SUMMARY

Continuous color polymorphisms can serve as a tractable model for the genetic and developmental architecture of traits. Here we investigated continuous color variation in *Colias eurytheme* and *Colias philodice*, two species of sulfur butterflies that hybridize in sympatry. Using quantitative trait locus (QTL) analysis and high-throughput color quantification, we found two interacting large-effect loci affecting orange-to-yellow chromaticity. Knockouts of *red Malpighian tubules* (*red*), likely involved in endosomal maturation, result in depigmented wing scales. Additionally, the transcription factor *bric-a-brac* can act as a modulator of orange pigmentation. We also describe the QTL architecture of other continuously varying traits, together supporting a large-X effect model where the genetic control of species-defining traits is enriched on sex chromosomes. This study sheds light on the range of possible genetic architectures that can underpin a continuously varying trait and illustrates the power of using automated measurement to score phenotypes that are not always conspicuous to the human eye.

INTRODUCTION

Color polymorphisms play key roles in adaptation and sexual selection in plants and animals[1–3] and provide a tractable system for the study of genotype-to-phenotype variation in natural populations.[1,4] Phenotypic diversification and divergence in the colors of natural populations can vary discretely and be linked to one or few large-effect loci, such as skin color in wall lizards,[5] plumage color in siskins and canaries,[6] or scale colors in *Heliconius* butterflies.[7] Elsewhere, color may vary continuously. Continuous color traits have often been linked to polygenic architectures consisting of many small-effect loci—for example, human hair color,[8] cichlid fish pigmentation,[9] or blue iridescence in butterflies[10,11]—with few studies addressing polygenic architectures with diverse gene effect sizes. In the era of falling sequencing costs and big-data phenomics, study of continuous color polymorphisms could provide fertile ground for improving our understanding of the genetic architecture of continuous traits.

A large number of studies have described the Mendelian genetics of color variation in animals and plants. Various modes of color production have been investigated, including the synthesis and deposition of melanin, carotenoid, psittacofulvin, and biliverdin pigments in vertebrates[12]; melanin, ommochrome, and pterin pigments in insects[13,14]; and the differentiation of iridescent structural features.[15] These Mendelian color polymorphisms have often been linked to a set of "hotspot" pigmentation genes that were first described in model organisms, such as *MC1R* and *agouti* for melanin variation and *BCO2* for carotenoids.[6,12]

More recently, studies in non-model organisms have identified new genetic mechanisms that underpin color variation, independent of the need for a candidate gene approach. This is exemplified by the identification of recently described enzymes Cyp2J19 and BDH1L in the carotenoid biosynthesis pathway, where a combination of genome-wide association studies (GWASs), quantitative trait locus (QTL) mapping, and functional validation illustrated that these enzymes convert dietary carotenoids into red ketocarotenoids in birds,[16] and have likely acquired their role in body pigmentation through regulatory co-option from their function in eyes.[17] Continuing broad surveys of color diversity are likely to uncover additional novel mechanisms for pigmentation across the Tree of Life.

Mendelian color loci have made excellent systems for studying the genetic architecture of variation in natural populations, allowing for preliminary assessments of common classes of mutation; for example, spatial variation in pigmentation is found to be caused by *cis*-regulatory variation more often than coding variation,[12] and signaling molecules such as ligands and their receptors are recurring mutational targets of color pattern evolution.[18] While these findings inform our general understanding of the genetic architecture of other Mendelian traits, most observable traits in wild populations are not Mendelian. Robust studies of continuous color variation are also needed to reflect the

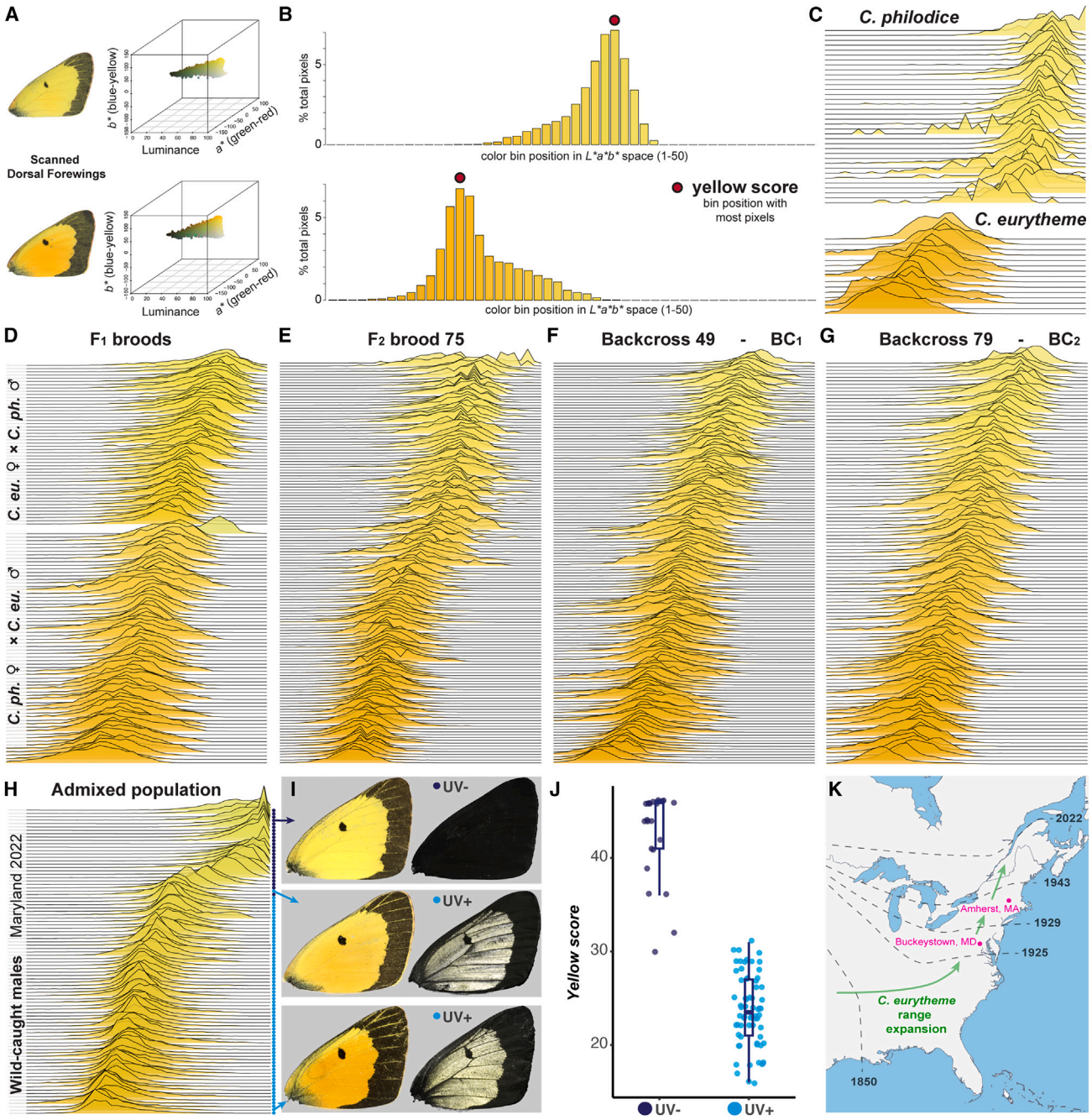

Figure 1. Rapid, repeatable, and automated phenotyping of wing color

(A) We used the package *r/colordistance* to extract pixel *L*a*b** coordinates from scanned wing images, followed by appropriate thresholding to remove background information; here we depict two representative males from the F_2 brood. We then selected a subset of the remaining pixel range to capture the orange-yellow region of CIELAB color space and divided it into 50 bins along the *b** axis.

(B) Pixel density histograms for the two individuals shown in (A), with color profile bin positions on the x axis. Bar colors correspond to the average color of each plotted bin and recapitulate the range of orange-to-yellow pixels of interest in further analyses. The bin with the maximum pixel count is hereafter referred to as "yellow score."

(C–G) Color binning profiles of every individual from the offspring of wild-caught individuals (C) and indicated broods (D–G).

(H and I) Wild-caught males from an agricultural site where *C. philodice* and *C. eurytheme* fly together and hybridize; the colored dots indicate the presence or absence of UV iridescence, allowing inference of the Z chromosome genotype.[40]

(legend continued on next page)

predominance of more complex traits that are pervasive in nature.[19] Continuous color polymorphisms provide an opportunity to observe how spectra of allele effect sizes can vary in different evolutionary contexts. It is common in the wild,[20,21] and can evolve rapidly in response to environmental perturbation.[22] Theoretical models predict that a combination of large-effect and small-effect loci will evolve in response to selection.[23] A study of *Drosophila melanogaster* abdominal melanization found that three large-effect loci explain one-third of color heritability, with as many as 17 additional smaller-effect variants contributing[24]; a similar architecture seems to be at play among two other, recently diverged *Drosophila* species.[25,26] Similarly in zebra finches, beak redness depends on environmental interactions, but has a heritable component that is partially explained by four linkage groups.[27,28] In contrast, in the polygenic white head patch of *Ficedula* flycatchers, no large-effect loci contribute to color, meaning the phenotype is inherited via many small-effect loci.[29] Identification of the causative genetic loci for continuous traits is complex when contrasted to Mendelian loci, as larger sample sizes and precise phenotype scoring methods are required to detect loci.[10,19,29] These challenges are highlighted by studies of skin and eye color variation in human populations, where large sample sizes are required to resolve genome-wide association signals due to small effect sizes and complex ancestries in the datasets.[30–32]

Here, we use North American *Colias* butterflies to determine the genetic architecture of continuous variation in pterin-based color in the wild. Pterin pigments are guanosine triphosphate (GTP) metabolites that are often co-opted to create bright reds, oranges, and yellows in a range of phylogenetically diverse animals.[33] As they constitute the red pigments in *Drosophila* eyes, the metabolic pathway has been well described through mutagenesis screens, although key steps in the pathway, including the hypothesized enzyme that converts xanthopterin to erythropterin, are not yet identified.[34] Further, there has been limited study of genetic variation in pterin pigmentation in wild populations, with natural allelic variants only identified so far in the mapping of discrete switches among color morphs of *Podarcis* lizards and the Alba morph of *Colias* butterflies.[5,35]

Colias exhibit a range of phenotypes that vary between a closely related species pair. *Colias eurytheme* display orange pterins and *Colias philodice* yellow pterins,[36,37] while females of both species carrying the low-frequency *Alba* polymorphism are white due to the suppression of pterin granules in their wing scales.[35,38] This species pair is in secondary sympatry in the eastern United States, where they undergo extensive hybridization in high-density agricultural sites, resulting in continuous variation in their pterin coloration.[39] These visible color differences are accompanied by a number of other segregating phenotypic differences, including the Mendelian-inherited presence or absence of UV iridescence,[40,41] as well as variation in size,[42] pheromones,[43,44] and mate preference.[45] Notably, these phenotypes have all previously been described as sex linked, indicating that the Z chromosome has a large effect in driving between-species differences. Consistent with a large-X effect,[46] a recent analysis of between-species differentiation showed a notably large divergence ratio between the Z chromosome and autosomes, although some evidence for diversification on the autosomes was also detected.[40] However, the number of alleles or effect sizes, including the role for autosomal inheritance in this system, has not been investigated.

In this study, we examined color variation in laboratory crosses of *C. philodice* and *C. eurytheme* using an automated image analysis pipeline across 705 butterflies, and we found extensive quantitative variation in visible pterin-based color. Using a previously published 2b-RAD linkage map for 483 individuals from F_2 and backcross (BC) broods, we mapped two large-effect QTLs that interact and jointly explain 70% of the observed wing color variation, including linkage to an autosome and the Z sex chromosome. We identified two candidate genes that modulate pterin color output upon CRISPR mosaic knockout (mKO). Finally, we measured other features of wing morphology, including size and pattern elements, finding these traits to similarly be polygenic but with evidence of linkage to the Z chromosome, supporting a model in which the sex chromosomes play an outsized role in the phenotypic diversification between incipient species.

RESULTS

High-throughput color analysis of yellow-orange color variation in interspecific crosses

We previously generated and genotyped a large cohort of *Colias eurytheme* × *philodice* laboratory crosses in Amherst, MA, in 2000–2002 and used these data to map the genetic basis of UV coloration, a discrete and male-specific trait.[40,47] These genotype data from 483 individuals in hand, we expanded on this resource to derive wing color and morphometrics continuous data by scanning and phenotyping the wings from a total of 705 butterflies, adding additional phenotypic data from F_0 parental populations of *C. eurytheme* and *C. philodice* as well as the offspring from two reciprocal F_1 crosses, an F_2 intercross, and two backcrosses to *C. eurytheme* females of F_1 males of reciprocal ancestries. Automated color measurements were taken for all four wing surfaces of all individuals. We sampled all pixel values in $L^*a^*b^*$ color space and applied threshold filters to eliminate pixels outside of the yellow-red portion of the spectrum. Noting that the axis with maximum variation was b^*, we subdivided the b^* axis into 50 bins (a stable subdivision of the total space), and counted the percentage of pixels that fell within each bin[48] (Figures 1A and 1B). Because of the multidimensional nature of $L^*a^*b^*$ color values, we simply recorded the ''yellow score'' as the modal bin position (i.e., having the most pixels on the color profile). The yellow scores of the dorsal and ventral forewing, as well as the dorsal hindwing, were highly correlated, while its values showed low variance in the ventral hindwings,

(J) UV-positive males are consistently more orange, while UV-negative males are consistently yellower.
(K) Summary of the northward expansion of *C. eurytheme* across the eastern US after 1850, as previously documented.[49] The eastern US comprised part of the native range of *C. philodice* before 1850. Parental admixed populations used for QTL mapping (C–J) originated from Amherst, MA (Summer 2000). Wild-caught males (H and I) were collected in Buckeystown, MD (August-September 2022).

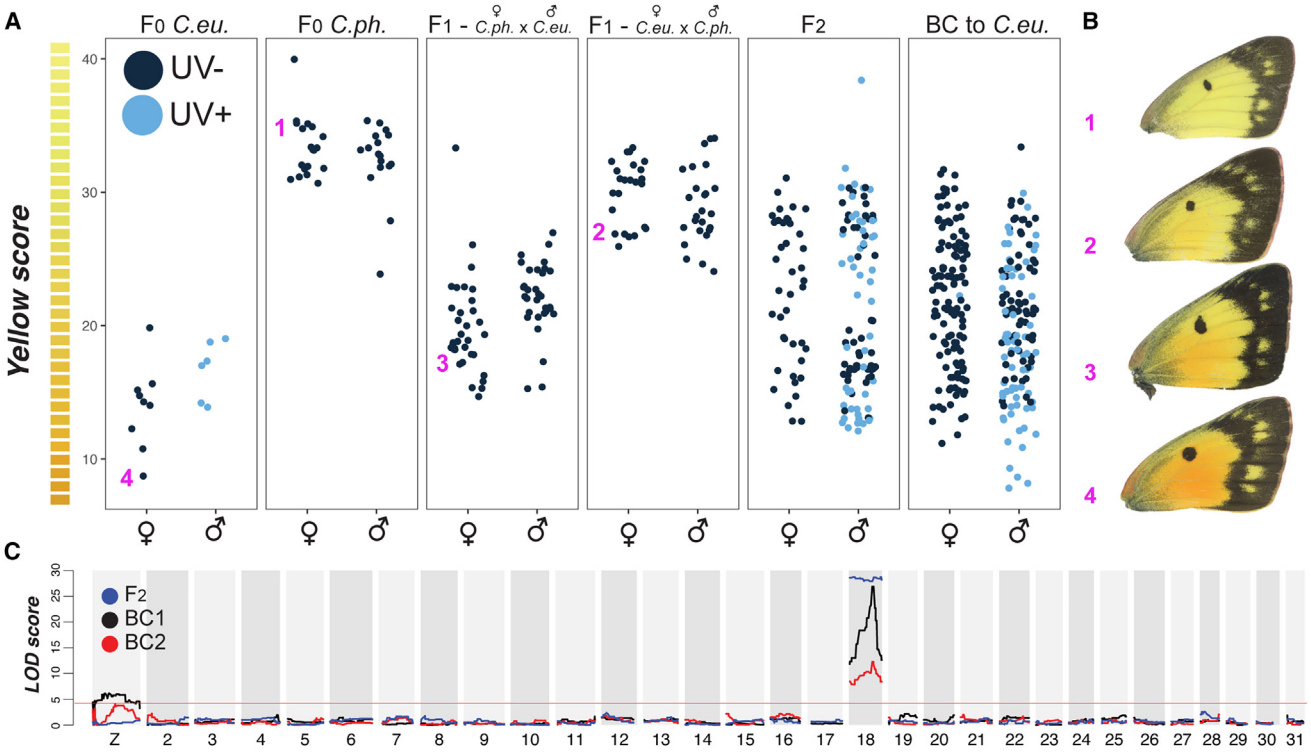

Figure 2. Yellow-orange color variation is linked to chromosome 18 and the Z sex chromosome

We measured yellow scores for all individuals from one F_2 and two backcross broods, as well as for a random subset of individuals from grandparental F_0 and parental F_1 broods. F_1 and F_2 broods show intermediate color between the parental broods.

(A–C) Four exemplar individuals from different parts of the color range are depicted in (B). We used these yellow scores as the input into QTL analyses, and found an LOD interval on chromosome 18 for all three broods, as well as LOD interval on the Z chromosome in both backcross broods (C).

where it was decoupled from the three other wing surfaces (Figure S1A). As such, we used dorsal forewing yellow scores for all further analyses (Figures 1C–1G and 2).

As expected, parental F_0 broods from wild-caught Massachusetts females had color values at each end of the range (Figures 1, 2A, and 2B). Offspring *C. philodice* siblings were yellower (yellow score 32.9 ± 2.5) and *C. eurytheme* siblings were oranger (yellow score 15.1 ± 3.1; Mann-Whitney U test, $p = 2.3 \times 10^{-8}$). The mean color of F_1 broods was dependent on the direction of the cross (Figure 1D); offspring with a *C. eurytheme* father were skewed to the orange end of the distribution (skewness of −0.12), while individuals with a *C. philodice* father were skewed to the yellow end of the distribution (skewness of +0.42). Similarly, F_2 and BC broods showed an intermediate distribution between the parental phenotypes (Figures 1E–1G). These trends replicate previous observations and suggest a contribution of the male-inherited Z sex chromosome to color.[42]

Random sampling of genetically unrelated males at a high-density agricultural site in Buckeystown, Maryland, exhibited a similar bimodal distribution in yellow score with few intermediates (Figures 1H–1K). This said, the UV-iridescence characteristic of *C. eurytheme* males is a recessive Z-linked character, allowing us to determine the genotype of the Z chromosome in these individuals from phenotype.[40,41] Wild-caught Maryland UV-positive males (i.e., carrying two *C. eurytheme* Z chromosomes) had a yellow score of 23.7 ± 3.8, while wild-caught UV-negative males (either one or two *C. philodice* Z chromosomes) had significantly yellower score of 42.8 ± 4.7 (Mann-Whitney U test, $p = 2.3 \times 10^{-13}$). Taken together, phenotypic data from laboratory crosses and an admixed population in field conditions both suggest the orange-yellow variation is a bimodal species-diagnostic trait and that its control is at least partially sex linked. We previously described a large-X effect that caused a strong differentiation of the Z chromosome haplotypes in the Maryland population, limiting genetic resolution by association mapping on this linkage group.[40] We thus focused on QTL mapping using laboratory crosses, where both autosomes and the Z chromosome have undergone significant recombination in F_1 hybrid males.[38,40]

Single QTL scan reveals an autosomal large-effect locus and a sex-linked modifier locus

We calculated an estimate for the effective number of genetic loci required to explain heritability and variance in yellow score using the Castle-Wright estimator, giving an estimate of 3.7 loci; this is likely an underestimate of the true number as it assumes all loci have equal effect size, but it suggests a model with fewer loci of moderate-to-large effect is likely.[50,51] Yellow scores were used as phenotypes for a single QTL analysis, with each brood analyzed separately. All three broods had a

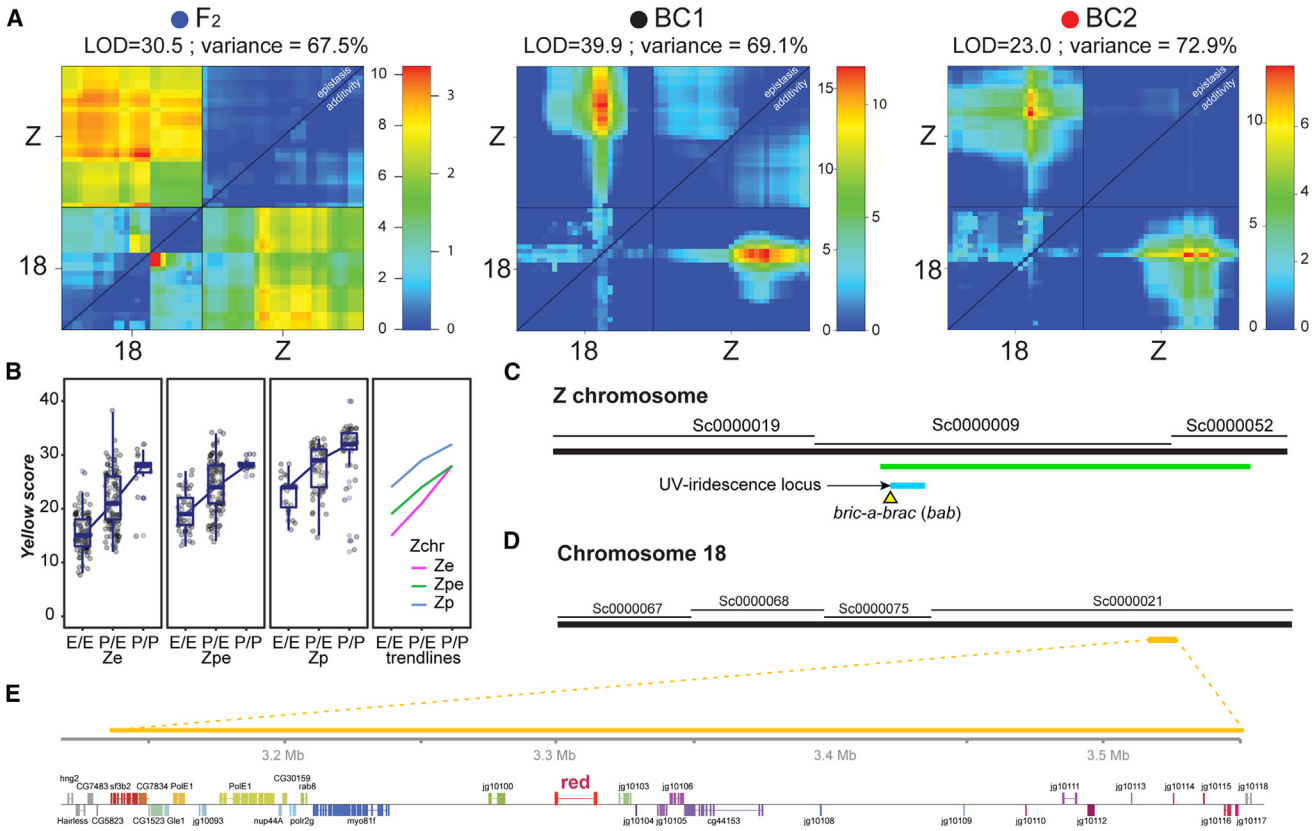

Figure 3. Additive interaction between the LOD intervals on chromosome 18 and the Z chromosome

(A) Two-QTL models for each brood indicate a significant interaction between the Z chromosome and chromosome 18. For each plot, the top left corner is the full model (two-QTL model plus interaction) and tests for epistasis, whereas the lower right tests for additivity among loci (two-QTL without interaction). Each color scale indicates two separate LOD scores for epistasis (left) and additivity (right). Significance threshold is set at 4.7 based on previous recommendations.[52]

(B) Genotype × phenotype plots showing the relationship between the Z chromosome genotypes (*Ze* and *Zp*, homozygotes or hemizygotes; *Zpe*, heterozygotes) and chromosome 18 LOD interval genotype (x axis) on yellow score. The rightmost panel overlays the means for the first three panels.

(C) The Z chromosome includes the *U* locus (cyan) for UV iridescence.[40]

(D and E) The LOD interval on chromosome 18 (yellow) is centered on the gene *red Malpighian tubules* (*red*).

significant QTL on chromosome 18, with a narrow Bayes-credible interval (Figure 2C). Unlike the backcross broods, the F_2 brood LOD scores on chromosome 18 were flat and the predicted LOD interval incorporated the entire chromosome, indicating that no informative recombinants were detected in this brood. The single-QTL model also detected a marginally significant secondary QTL on the Z chromosome in the BC1 and BC2 broods (Figure 2D). It is notable that, despite the strong correlation between the Z-linked UV phenotype and yellow score in the Buckeystown wild-caught individuals, the linkage interval with the highest LOD score is autosomal. This, as well as the expectation of additional loci, prompted further dissection of the genetic architecture of color variation in our mapping panel.

A two-locus interaction explains 70% of color variation

To look for interactions and for other, smaller-effect loci, we fitted a two-QTL model to each brood separately. For each brood, we identified significant QTL on both chromosome 18 and the Z chromosome, which together explain about 70% of variance in yellow score (Figure 3A). At each QTL, individuals with *C. eurytheme* alleles had low yellow scores, individuals with *C. philodice* alleles had high yellow scores, and heterozygotes had intermediate yellow scores (Figure 3B). This additive effect is supported by the additive model (plotted below the diagonal in Figure 3A), which was significant in BC1 and BC2, but did not reach the genome-wide threshold of significance in the F_2 brood.

All three broods also show evidence for a significant interaction between the two LOD intervals as shown in the full conditional model (Figure 3A, above the diagonal). As indicated by the genotype × phenotype plot, when individuals are homozygous for the *C. philodice* allele at the chromosome 18 LOD interval, one copy of the *C. eurytheme* allele at the Z LOD interval makes them more orange, but two copies does not shift this any further. This deviation from the sum of the effects of the two loci indicates an epistatic interaction. To determine if additional smaller-effect loci could be detected, we ran multiple-QTL models that accounted for the two detected loci. No additional loci met the genome-wide threshold of significance.

The chromosome 18 LOD interval is 500 kb and contains 29 annotated genes (Table S1A), including a homolog of the gene *red Malpighian tubules* (*red*). The *red* gene is a compelling candidate gene for pterin pigment variation in butterflies, as mutant and knockdown phenotypes in *Drosophila* and *Oncopeltus* have suggested a role of this gene in the biogenesis of pigment granule formation, including pterinosomes.[53,54] No coding variants were detected in whole-genome-resequenced individuals from Buckeystown, MA.

The Z chromosome LOD interval encompasses a large portion of the chromosome and spans 270 genes (Table S1B), including the *U* locus interval with the *bric-a-brac* (*bab*) transcription factor gene, which determines male-limited UV-iridescence variation in *C. eurytheme* and *C. philodice*.[40,55] Interestingly, we previously reported unusual orange-yellow variation in *C. eurytheme* females following CRISPR mutagenesis of *bab*, prompting a more refined examination of this genetic effect and suggesting that *bab* controls both structural and pigment-based color differences between the two species.

Last, we ran a two-QTL model for the full dataset combining all three broods and detected a marginally significant interaction between chromosome 18 and chromosome 12, which was not observed in the analyses on separate broods. The chromosome 12 LOD interval incorporates 232 genes and explains 3% of variation in color (Figure S2; Table S1C).

mKOs of *red* disrupt pigmentation and intraluminal scale organization

In order to test a role of *red* in wing pterin modulation, we used CRISPR mutagenesis targeting a coding exon of *red* to generate null, mosaic mutant clones in G_0 injected individuals. A total of 305 syncytial embryos were collected from wild-caught *C. eurytheme* females and injected within 4 h after egg laying (AEL). From these injections, we obtained 27 emerged adult butterflies, 20 of which (74%) showed visible color changes in mutant clones (Figure 4; Table S1D). Both ventral and dorsal wing surfaces were affected, and mutant clones showed a gain of broad-spectrum (non-iridescent) UV reflectance (Figures S3 and S4), suggesting a decrease of UV-absorbing pterin pigments in mutant scales.[37,56] Dorsal hindwing discal spots, which normally display a deep orange color regardless of the species and sex, showed the most marked color shifts among crispants (Figure S5). Elsewhere on the wing, and most markedly on dorsal surfaces, the pale color of mutant clones somewhat resembled Alba female morphs but with a higher chromaticity (Figures S4A–S4K), implying that *red* knockouts (KOs) do not fully suppress pterin granule formation as observed in *Alba* genotypes.[35] To better characterize the effects of *red* loss of function on wing chromaticity, we digitized crispant wings in constant conditions and then analyzed wild-type (WT) and mutant clones in immediately adjacent patches of wing in CIELAB color space (Figures 4I–4K). WT populations show little variation in luminance (L^*), but *C. eurytheme* has higher a^* values (i.e., they are redder) and b^* values (i.e., they are also yellower) than *C. philodice*. Crispant clones consistently showed a small reduction in a^* and remained above the *C. philodice* states, while b^* values fell under the *C. philodice* values. This overall reduction in chromaticity suggests a decrease in the pterin content of *red* crispant wings, akin to but less drastic than in Alba females.[35]

In pierid butterflies, pterin pigment granules (pterinosomes) can be directly visualized by scanning electron microscopy (SEM). Pterinosomes normally form oblong ellipsoid structures attached along the transversal trabeculae of the upper scale surface and suspended in the hollow scale matrix.[36] This organization was disrupted in *red* crispant scales, which showed a normal organization of the scale outer structures but a chaotic mesh of interwoven structures in their inner part (Figure 5). Pterinosomes were apparent but scarce and disorganized, likely explaining the residual chromaticity in these scales, and fused with other chitinous elements. Under the hypothesis that pterinosomes are lysosome-related organelles that derive from the scale endomembrane system,[57,58] these phenotypes are consistent with a disruption of intraluminal organelle maturation or trafficking.

The UV-iridescence switch gene *bab* is also a candidate gene for pterin variation

Our two-QTL scan identified a large portion of the Z chromosome as a secondary locus interacting with chromosome 18, with a confidence interval that includes the *U* locus, previously described in Ficarrotta et al.,[40] which contains the causative gene *bab*. *C. eurytheme* and *C. philodice bab* crispant clones display spectacular gains of UV iridescence across all wing surfaces and in both sexes. Interestingly, we previously noticed that, while *bab* mKOs do not yield effects on human-visible color in males, *C. eurytheme* crispant females displayed noticeable heterogeneity in visible color.[40] We re-examined this phenomenon and found the *bab* loss-of-function clones resulted in context-dependent effects on several color traits in *C. eurytheme* females (Figure 6).

Observation of wings with a 30° light incidence highlighted a gain of an iridescent color, visible as a blue sheen on melanic scales and as a violet-pink sheen on orange scales (Figure 6C′). This effect is limited to females and is likely an effect of UV-signal overflow in the visible spectrum following the gain of densely stacked ridges on the surface of the UV-iridescent scale type. As this iridescent color is angle dependent, we imaged these wings at a 0° incidence as well as with polarized light-reflected microscopy to rule out this ectopic iridescence as having an effect on the appearance of pterin-based color (Figure 6C). Because mutant vs. WT clones maintained marked differences in orange-yellow pigmentation with these observation techniques, we infer that *bab* KO results in the modulation of pterin content in females, separately from its role in structural color.

Of note, *bab* crispant clones are marked by ectopic UV iridescence, allowing us to precisely delineate the boundaries of WT vs. mutant wing scales. On the dorsal wings, we found that *bab*-deficient clones show an increase in orange pigment compared to adjacent WT clones (Figures 6D and 6E). The analysis of ventral surfaces revealed a more nuanced picture, because the specific effect of *bab* mutagenesis on red pigmentation varied across the proximodistal axis (Figures 6F–6K′). In proximal regions, *bab* mutant clones showed redder pigmentation relative to adjacent WT clones, while, more distally, they were lighter, including in the most distal section of the wing where marginal scales that normally display pink pterins[59] were depigmented. In addition, *bab* mKOs resulted in an elongation of silver scales and darker melanization in the ventral discal spot (Figure S6).

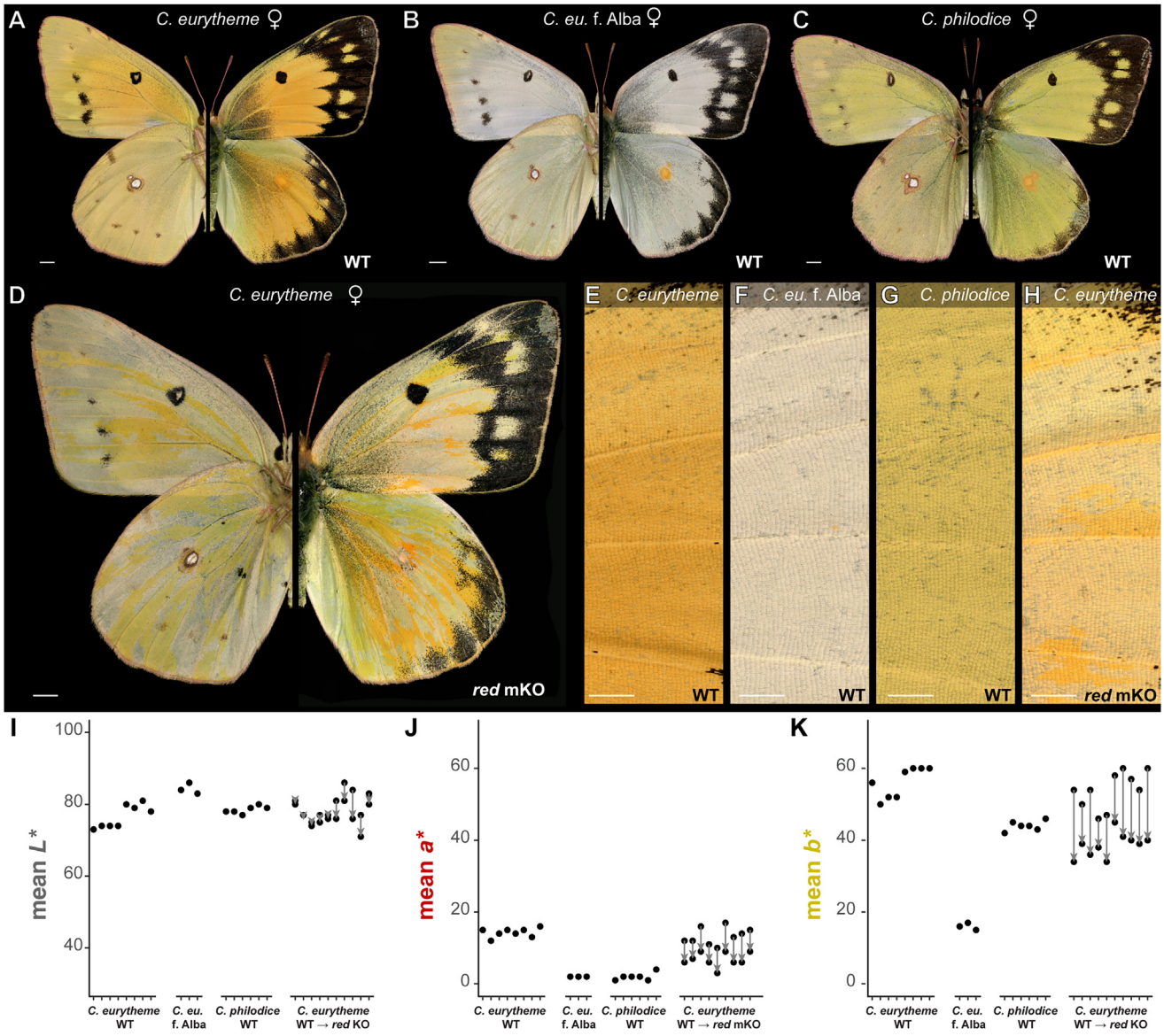

Figure 4. Wing coloration effects of *red Malpighian tubules* CRISPR mKOs

(A–C) Ventral (left) and dorsal of wild-type (WT) females representative of admixed *C. eurytheme* and *C. philodice* populations, here sampled from Maryland.

(D) *C. eurytheme* G_0 mosaic crispant for the *red* gene with discolored streaks (mutant clones) imaged in identical conditions to the WT controls.

(E–H) Side-by-side comparisons of dorsal forewing regions show reduced orange coloration in *red* KO clones (H) relative to *C. eurytheme* WT clones; compare to Alba individuals, which completely lack pterin granules.

(I–K) Comparison of mean *L** (luminance), *a** (green to red), and *b** (blue to yellow) pixel values sampled from dorsal WT forewings and from adjacent WT vs. *red*-deficient clones from 10 *C. eurytheme* crispants, contrasted to Alba individuals that lack pterins. Scale bars, (A–D) 2,000 μm, (E–H) 1,000 μm.

In summary, CRISPR KOs revealed *bab* is required for normal pterin pigmentation in females in a complex fashion, with *bab*-deficient clones showing increased orange pigmentation on dorsal surfaces and varying effects across the proximodistal axis on ventral sides. Allelic variation of the *bab* locus may thus explain all of the color variation linked to the Z chromosome LOD interval, possibly through the direct activation or repression of pigment pathway components, similar to its role in shaping *Drosophila* abdominal pigmentation via other interacting QTLs.[60–62] Alternatively, the sex-linked secondary QTL may be explained by other genes independent of *bab*. Traditional QTL mapping may be limited to test this possibility, as it might require the generation of many large recombinant broods controlling for *red* allelic states to properly extract a narrow signal on the Z chromosome.

Wing size is heritable and sex linked

Previous work showed that *C. eurytheme* were consistently larger than *C. philodice* and that this size difference was heritable and sex linked.[42,63] We quantified wing size, along with a number

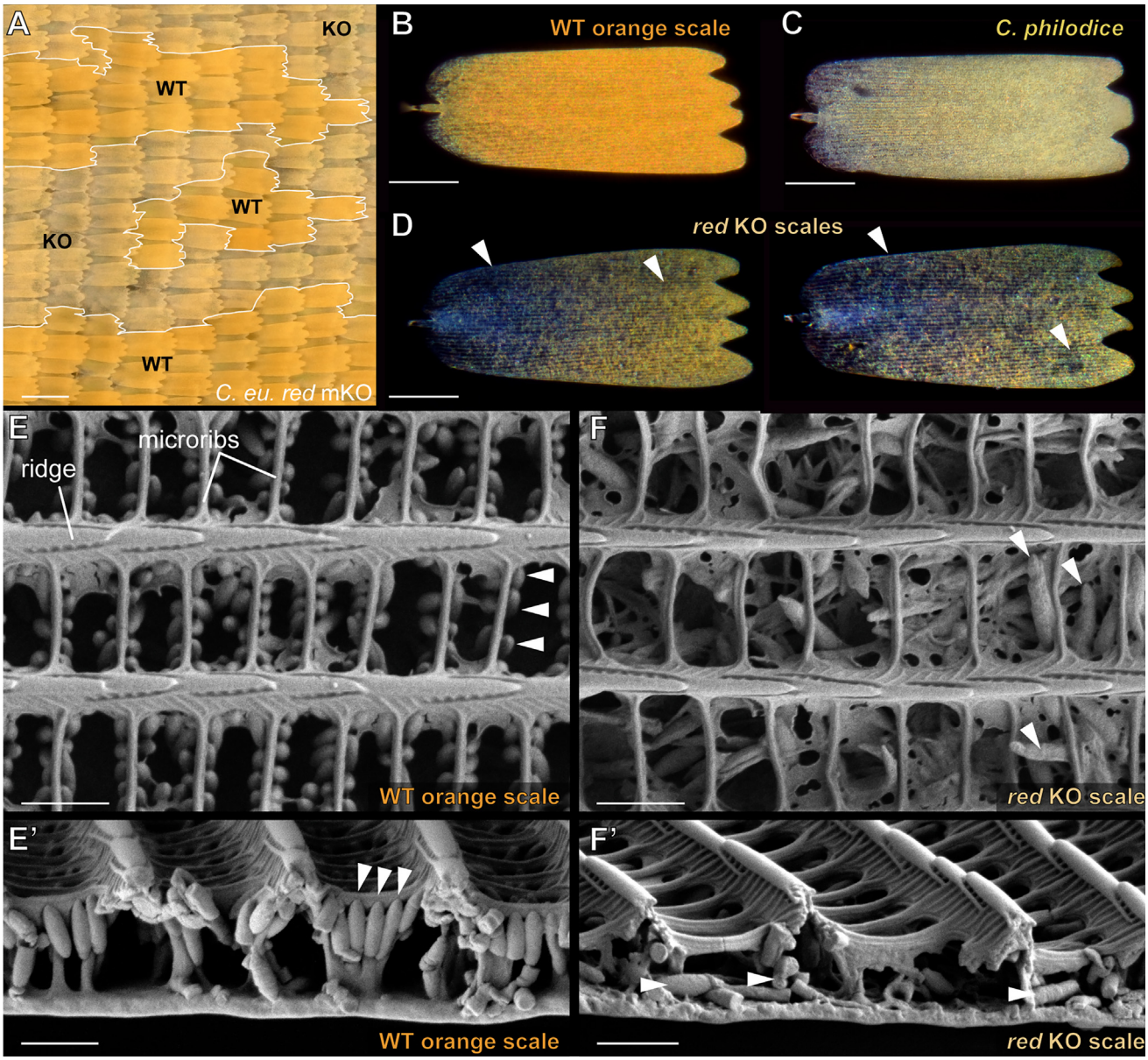

Figure 5. Disorganization of internal scale structures in *red* crispant scales

(A) Scale-level coloration of *red* mKO clones relative to WT phenotypes in *C. eurytheme*, here in dorsal forewing regions.

(B–D) Reflected polarized microscopy of individual dorsal forewing scales from a *C. eurytheme* female (B), a *C. philodice* female (C), and a female *C. eurytheme* *red* crispant clone (D). Scales from (B) and (D) are from adjacent clones in the same crispant individual. Scales deficient for *red* have poor refringence and show an overall lack of pigment density (arrowheads).

(E and E′) SEM top (E) and cross-sectional (E′) views of WT orange scales. Pterin granules (arrowheads) are visible as oblong structures attached to the microribs, the structures that form transversal bridges between the ridges of the scale upper lamina.

(F and F′) Defects of the inner scale lumen in *red* crispant scales, amid a normal upper surface. Pterin granules (arrowheads) are improperly formed, fail to attach to microribs, and are randomly arranged in a disorganized scale matrix. Scale bars, (A) 100 μm, (B–D) 50 μm, (E–F′) 1 μm.

of other morphometric measurements, including features of the discal spots and the marginal bands, from all 705 individuals (Figure S7). Principal-component analysis of all measures showed separation between UV-positive and UV-negative males in the first component, once again indicating a likely contribution from the sex chromosomes. Of note, we replicated a small but significant difference in wing length between females of the two parental species ($p = 0.03$, Wilcoxon test) (Figure 7).

The morphometric features we measured could have been controlled by the same or linked loci and might not be independent variables, so, in order to determine the co-inheritance of these traits, we performed a hierarchical clustering analysis to look for

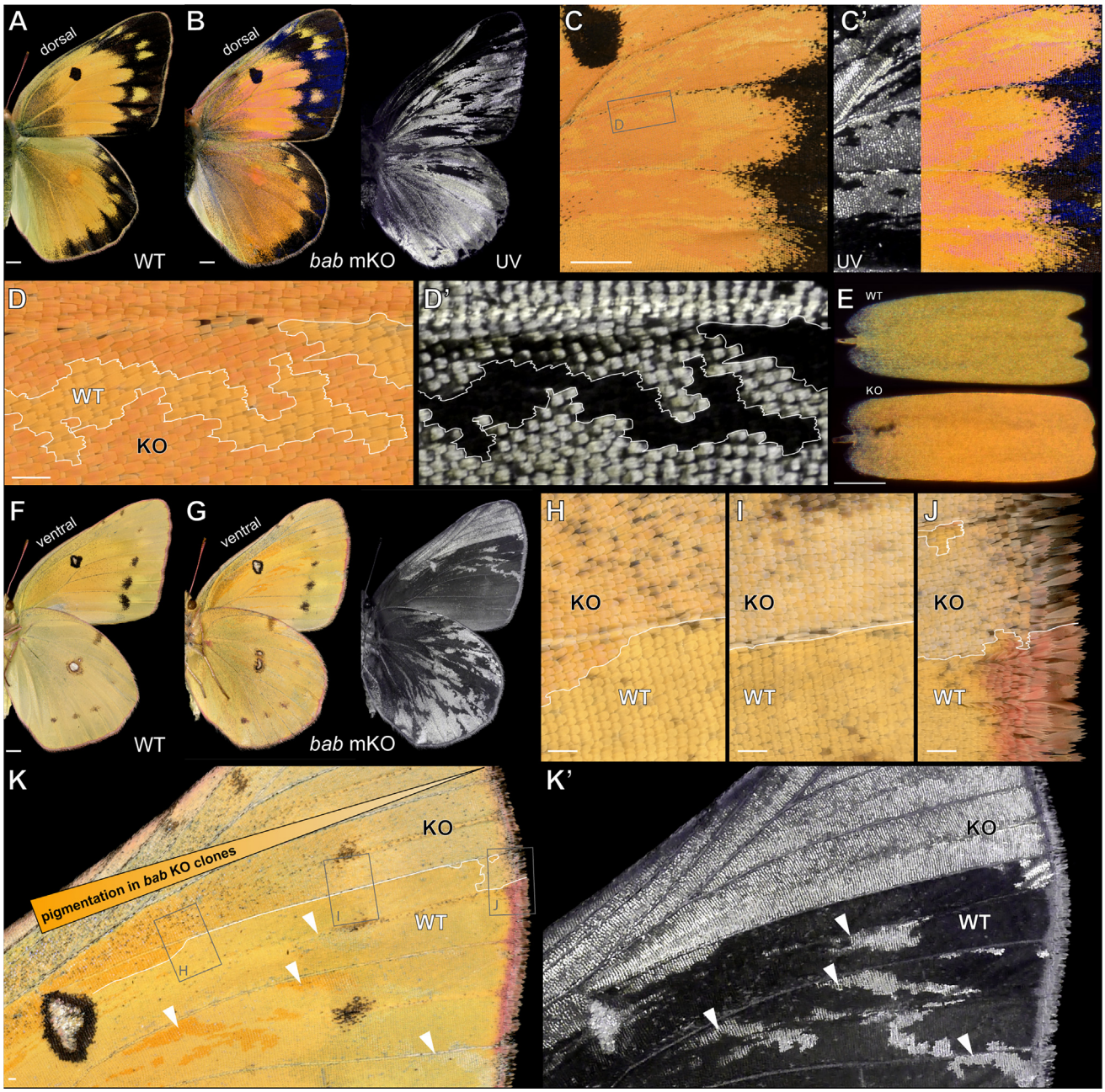

Figure 6. CRISPR mutagenesis of *bab* can affect both UV iridescence and pterin pigmentation

(A) WT *C. eurytheme* female, dorsal view.

(B–C′) Dorsal views of a *bab* crispant *C. eurytheme* female.[40] Crispant clones lacking *bab* display ectopic UV iridescence in all regions, ectopic blue iridescence over melanic regions, and color shifts in orange regions, with the two latter effects only observed in crispant females. (C) The visible-spectrum coloration with normal light incidence (0°); (C′) the structural iridescence effects in the UV-A and visible ranges observed with a 30° light incidence.

(D and D′) Magnified views of WT and KO *bab* crispant clones with 0° incidence.

(E) Polarized reflective microscopy of adjacent scales from across a *bab* crispant boundary.

(F) WT *C. eurytheme* female, ventral view.

(G–K′) Ventral views of a *bab* crispant *C. eurytheme* female. On the ventral surface, the effect of *bab* loss of function over pterin pigmentation changes over the proximodistal axis. Scale bars, (A, B, F, and G) 2,000 μm, (C, D and H–K) 200 μm, (E) 50 μm.

covariance between measurements. Our measured traits optimally split into five clusters, one each corresponding to size, forewing discal spot, hindwing discal spot, forewing and hindwing black margin thickness, and wing aspect. We then used the latent variable for each of these trait clusters for QTL analysis (Figures S8 and S9). Two significant LOD intervals for size were detected, on

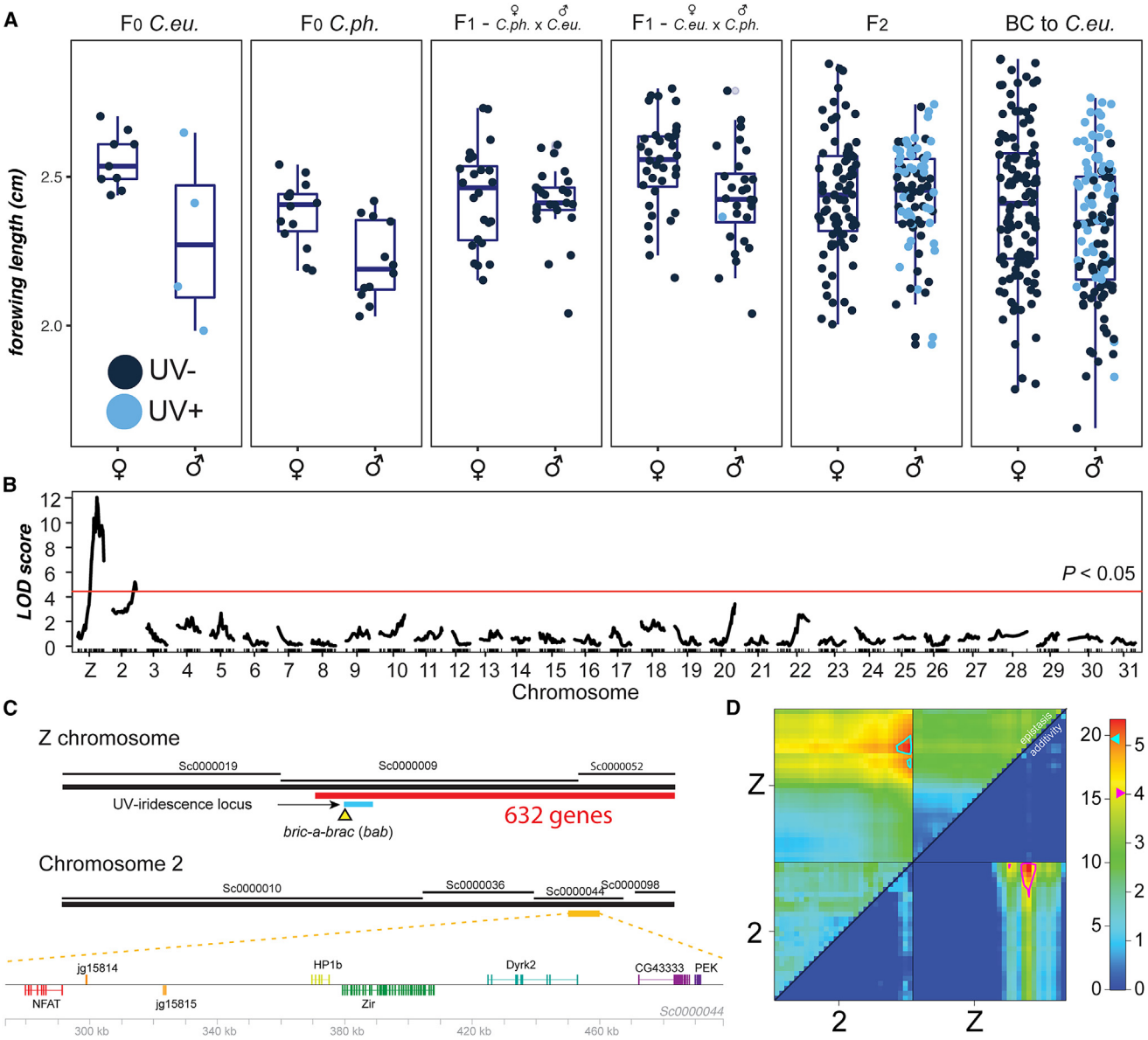

Figure 7. Two LOD intervals associated with wing size

(A) Variation in wing length in crosses.

(B and C) A single-QTL model detects two significant loci (B) that incorporate large portions of chromosome 2 and the Z chromosome (C).

(D) Support for an additive two-QTL model that explains 18% of the variation in size, with LOD scores for the full model on the upper left and for the additive model on the lower right.

the Z chromosome and on chromosome 2 (Figure 7). In a two-QTL model, an additive interaction between the two loci explained 18% of variation in size. Additional significant QTLs were also detected for the hindwing discal spot, the forewing discal spot, and the thickness of the black margin (Figure S8).

The Z-linked LOD interval for size incorporates around half of the chromosome and includes 638 genes, including the entirety of the LOD interval for color described above (Table S1B). The LOD interval for size on chromosome 2 was more compact, including eight genes (Figure 7C; Table S1E). Further linkage analysis or association studies would be required to allow the determination of candidate loci for variation between *C. eurytheme* and *C. philodice*; this trait is likely to be highly polygenic, reflecting their divergent life-history strategies for size and rate of growth.[42,63]

DISCUSSION

Phenotyping continuous color variation

We were able to rapidly and objectively score continuous color in many individuals, permitting us to identify the underlying genetic

architecture of an interspecific variable trait. There are significant challenges for these types of quantitative analyses that make this approach necessary; the human eye may not always detect all meaningful variation. Objective measurement of color may reveal real, mappable signals that are indistinguishable in the human vision model; for example, recent analysis of tiger moth wings has shown that automated measurements can detect heterozygotes where humans cannot, highlighting the importance of objective measures.[64] This is compounded by the requirement for large numbers of individuals for the mapping of quantitative traits; as we continue to map continuous traits in future, we will begin to encounter datasets with many thousands of individuals. To cope with big-data phenomics, we need an increased focus on developing methods that can allow rapid phenotypic characterization. Approaches such as the one used here for color measurement should be scalable in order to deal with very large and complex datasets.

The genetic architecture of yellow-orange color variation is oligogenic

We used interspecific laboratory crosses of *C. eurytheme* × *philodice*, two sulfur butterfly species that occur in secondary sympatry, to shed light on the genetic architecture of continuous wing traits, and we used a high-throughput color quantitation method to map the loci underlying the yellow-orange color characteristic of these species. We found that two large-effect loci and one small-effect locus together explain 73% of the heritable variance in yellow score and indicate a mostly oligogenic architecture. This result contrasts with general expectations that many loci of smaller effect should underlie quantitative trait variation,[19,65] as illustrated (using similar methodology and traits) by three additive QTLs that explained only 8% of the heritable variation in ornamental orange coloration in stickleback fishes.[66] Our epistatic QTL detected in the two-QTL scan were highly significant, although we may overestimate due to the Beavis effect.[67] This means that 27% or more of the color variance remains unaccounted for in our mapping panel, and it would require high statistical power from large crosses to identify further underlying small-effect loci.[4,19,68] The genetic epistasis that we identified here could potentially be explained by physical epistasis with the identified loci acting in the same pathway. This could include direct or indirect transcriptional regulation of downstream pigment synthesis genes by *bab*. Finally, yellow-orange variation is known to be seasonal[39,69,70] and correlated with a melanic trait that is influenced by day length across many pierids.[71–73] Here, our mapping approach controlled for genotype × environment effects as all broods were reared under constant conditions, but we expect variation in nature to include a more complex architecture, including loci that may modulate the responsiveness of chroma to photoperiod, temperature, or larval nutrition.[74,75] It is therefore probable that the effect sizes we observed for these loci under constant conditions are larger than they would be when variation in environmental conditions recruits additional loci that contribute to phenotypic variation.

red Malpighian tubules: A candidate regulator of pterinosome maturation

In this study, mapping and mKO experiments implicated the homolog of the fly *red* gene as a large-effect QTL controlling color variation between sympatric *Colias* species. This gene encodes a protein with a conserved LysM domain, although its molecular function has seldom been studied. The *Drosophila* mutant strain *red Malpighian tubules* (*red*) was described in 1954[76] and has been used as a marker gene,[77,78] but its molecular annotation to the *red* coding gene was only recently described.[54] Of the 21 genes in the chromosome 18 QTL, *red* is the only gene with a previously described role in pigmentation,[53,54] so it is possible but unlikely that other genes within this interval contribute to its effect on pigmentation.

This said, several lines of evidence point to *red* as a gene involved in the trafficking and maturation of pigment granules, which are endosomal compartments known as lysosome-related organelles (LROs), and are universally involved in pigment processing throughout animals.[14,57,79] The *D. melanogaster red* mutant shows an accumulation of red ommochromes in the Malpighian tubules (MTs) and a reduction of ommochromes and pterins in the eyes.[80–82] In the milkweed bug *Oncopeltus fasciatus*, RNAi-mediated knockdown of *red* causes a reduction in pterins in pigmented cuticles, legs, and abdomens, as well as a reduction of ommochromes in the eye.[53] Wing pigmentation is primarily pterin based in *Colias*, with no contribution from ommochromes,[37] but the dual effects on both ommochromes and pterins in *Drosophila* and *Oncopeltus* suggest that *red* acts at the level of a biological process that is shared between these pathways. Importantly, *red* mutant MTs show aberrant vesicular phenotypes that imply a failure of pigment granules to properly mature and excrete their content in the lumen.[82] These effects are reminiscent of other eye color mutant genes of the "granule group," which are required for the biogenesis of LROs, including ommochromasomes and pterinosomes.[13,14,83] In our SEM analysis of *red* crispant scales, we observed defective and disorganized pterinosomes amid otherwise normal scale morphologies (Figure 5). While further work is needed to establish the cellular roles of this gene, these data collectively suggest that *red* is involved in the trafficking or maturation of pigment granules, including pterinosomes and ommochromasomes.

In addition, a few observations lead us to speculate that *red* may regulate pigment granule activity by interacting with the vacuolar pH of pigment granules. First, the unique pigment profile of *red* mutant flies is strikingly similar to the ones observed with two eye-color mutant alleles of the *chocolate (cho)/VhaAC39* gene,[54,81,84] which encodes a v-ATPase proton pump essential for endosomal acidification and membrane trafficking in LROs.[85–87] Second, homologs of Red contain a LysM domain, and it is their only annotated feature.[53,54] The molecular function of this domain is poorly understood in insects, but there is mounting evidence in vertebrates that the LysM domains of several genes interact with the v-ATPase to modulate vacuolar pH across a variety of endosomal organelles.[88–91] There is precedent for a role of pterinosome acidification in modulating the red vs. yellow states of squamate pigment cells,[92] and the roles of melanosomal pH and v-ATPase activity in fine-tuning melanin content are well established in vertebrates.[93,94] Thus, while future work will be needed to dissect the roles of insect *red* and *cho* in v-ATPase function in pigment granules, we speculate that *red* regulates pterin composition by modulating the pterinosome vacuolar pH in *C. eurytheme* and *C. philodice*.

Evidence for a "species-defining" sex chromosome

The North American sulfur butterflies *C. philodice* and *C. eurytheme* co-exist in sympatry while maintaining effective reproductive barriers,[47] and the Z sex chromosome plays a disproportionate role in keeping these species distinct, an effect known as the large-X effect.[46] Moreover, the Z chromosome has a remarkably high level of divergence compared to autosomes,[40] and it also acts as a large linkage group coupling key reproductive barrier traits such as asymmetric hybrid female sterility, both male pheromone signal and female preference, as well as male UV signal and female preference; it thereby acts as a cluster of loci involved in incipient speciation.[42–45] The UV coloration signal, a recessive marker that distinguishes *C. eurytheme* males from hybrids and allows conspecific females to find compatible gametes, is explained by allelic variation of the *bab* transcription factor, a suppressor of UV scales that is specifically de-repressed in a small fraction of cells in iridescent males. Here, we showed that two additional traits that vary between this species pair, pterin coloration and wing size, are also linked to the Z chromosome. CRISPR KOs implicate a role for *bab* in orange-yellow pigmentation. It thus represents a good candidate gene for regulating interspecific variation, although, given the large size and gene content of the mapped QTL, the causative variants may in fact be associated with another gene in the interval. A sexual signaling role of dorsal visible color (orange vs. yellow) is unlikely in males and untested in females.[55] While this is also untested, wing chroma differences may have been shaped by ecological adaptation to climatic differences in the native ranges of *C. eurytheme* vs. *C. philodice*,[49] as suggested by the seasonal plasticity of this trait.[39,59] Wing size differences (a proxy for total body size) are likely to reflect the divergent life history of these butterflies, with *C. philodice* reaching pupation faster than *C. eurytheme* despite identical growth rates on their introduced host plants.[63]

The accumulation of LOD intervals for species-defining traits on the Z chromosome suggests that the Z chromosome could be behaving like a chromosome-wide supergene. It is possible that few linked large-effect loci under strong selection, plus the 0.75× recombination rate on sex chromosomes vs. autosomes, can more easily overcome the effects of introgression in comparison to autosomes,[95,96] as corroborated by the strong signature of Z chromosome differentiation between the two *Colias* species in sympatry. On the other hand, we have described additional autosomal loci that have persisted in divergence between the two species, including for size, color (i.e., *red*), and additional phenotypes (Figure S8). This coupling between the Z chromosome and autosomes could represent the remnant of eroding barrier loci or be the a signal of the persistence of stable ecomorphs maintained in part by sexual selection.[97,98] The resulting genetic architecture, with comparatively few loci contributing a large effect to a continuous trait, bears similarity to other described cases of color variation, including blue iridescence in butterflies and plumage color in capuchino seedeaters where a few large-effect loci explain a high fraction of variance,[10,99] while standing in contrast to other cases where many smaller-effect loci predominate, including the white head patch of *Ficedula* flycatchers.[29] This adds to a growing picture of the genetic control of continuous traits.

Limitations of the study

While our QTL mapping and CRISPR studies identify two candidate genes involved in wing color tuning, it remains unclear if they bear allelic differences that drive the color differences between *C. eurytheme* and *C. philodice* (for example, by driving expression differences between allelic states). It remains to be seen when—or if—allelic differences at the *red* locus result in consistent measurable differences in gene expression. In the future, it will be interesting to conduct transcriptional studies spanning a dense time series of both species. This would confirm differential expression and allow us to rule out any potential contributions from other genes in the LOD intervals.

Additionally, while our imaging and microscopy describe color variation accurately, this does not provide any information on what components of the pterin pigment content are responsible for this variation between species and in mutants, or the mechanism by which our identified loci impinge on pterin synthesis. This study thus prompts future detailed biochemical characterization of pterin content differences between the two species, with possible investigations of vacuolar pH on pterin maturation. Our experimental broods were all reared in standard controlled conditions; in the field, it is likely that the loci we mapped would be interacting with photoperiod and temperature in ways that remain un-quantified.

STAR★METHODS

Detailed methods are provided in the online version of this paper and include the following:

- KEY RESOURCES TABLE
- RESOURCE AVAILABILITY
  - Lead contact
  - Materials availability
  - Data and code availability
- EXPERIMENTAL MODEL AND STUDY PARTICIPANT DETAILS
  - Butterfly mapping broods
  - Butterfly mosaic KOs
  - Larval host plants
- METHOD DETAILS
  - Color imaging
  - CRISPR mutagenesis
  - UV macrophotography and microphotography
  - Scanning Electron Microscopy
  - Image post-processing
- QUANTIFICATION AND STATISTICAL ANALYSIS
  - Automated color scoring
  - Landmarking, morphometrics and clustering analysis
  - QTL analysis and gene identification
  - Colour-enhanced figures

SUPPLEMENTAL INFORMATION

Supplemental information can be found online at https://doi.org/10.1016/j.celrep.2023.112820.

ACKNOWLEDGMENTS

We thank Baiqing Wang for previously generating mapping broods,[100] Vincent Ficarrotta for previously generating *bab* crispants used in this study,[40] Scott Barao and Hedgeapple Farm (Buckeystown, MD) for providing access to alfalfa fields, the GW Nanofabrication and Imaging Center for SEM access, Rachel Canalicchio and the Wilbur V. Harlan Greenhouse staff for host plants, and the Research Technology Services at the George Washington University for operating the High Performance Computing Cluster.[101] We thank the Martin lab for their comments on this paper.

This work was funded by the National Science Foundation (IOS-1755329), and Harlan Foundation summer fellowships to O.B.W.H.C. and L.S.L.

AUTHOR CONTRIBUTIONS

Conceptualization, J.J.H., A.H.P., and A.M.; investigation and formal analysis, J.J.H., C.M.F., O.B.W.H.C., and L.S.L.; data curation, O.B.W.H.C., M.A.N., and D.J.L.; visualization, J.J.H. and A.M.; writing, J.J.H., A.H.P., and A.M.

DECLARATION OF INTERESTS

The authors declare no competing interests.

INCLUSION AND DIVERSITY

One or more of the authors of this paper self-identifies as an underrepresented ethnic minority in their field of research or within their geographical location. One or more of the authors of this paper self-identifies as a member of the LGBTQIA+ community. One or more of the authors of this paper self-identifies as living with a disability. While citing references scientifically relevant for this work, we also actively worked to promote gender balance in our reference list.

Received: February 14, 2023
Revised: June 2, 2023
Accepted: June 29, 2023

REFERENCES

1. Orteu, A., and Jiggins, C.D. (2020). The genomics of coloration provides insights into adaptive evolution. Nat. Rev. Genet. *21*, 461–475.
2. Sapir, Y., Gallagher, M.K., and Senden, E. (2021). What Maintains Flower Colour Variation within Populations? Trends Ecol. Evol. *36*, 507–519.
3. Wellenreuther, M., Svensson, E.I., and Hansson, B. (2014). Sexual selection and genetic colour polymorphisms in animals. Mol. Ecol. *23*, 5398–5414.
4. San-Jose, L.M., and Roulin, A. (2017). Genomics of coloration in natural animal populations. Philos. Trans. R. Soc. Lond. B Biol. Sci. *372*, 20160337.
5. Andrade, P., Pinho, C., Pérez I de Lanuza, G., Afonso, S., Brejcha, J., Rubin, C.J., Wallerman, O., Pereira, P., Sabatino, S.J., Bellati, A., et al. (2019). Regulatory changes in pterin and carotenoid genes underlie balanced color polymorphisms in the wall lizard. Proc. Natl. Acad. Sci. USA *116*, 5633–5642.
6. Gazda, M.A., Araújo, P.M., Lopes, R.J., Toomey, M.B., Andrade, P., Afonso, S., Marques, C., Nunes, L., Pereira, P., Trigo, S., et al. (2020). A genetic mechanism for sexual dichromatism in birds. Science *368*, 1270–1274.
7. Westerman, E.L., VanKuren, N.W., Massardo, D., Tenger-Trolander, A., Zhang, W., Hill, R.I., Perry, M., Bayala, E., Barr, K., Chamberlain, N., et al. (2018). Aristaless Controls Butterfly Wing Color Variation Used in Mimicry and Mate Choice. Curr. Biol. *28*, 3469–3474.e4.
8. Morgan, M.D., Pairo-Castineira, E., Rawlik, K., Canela-Xandri, O., Rees, J., Sims, D., Tenesa, A., and Jackson, I.J. (2018). Genome-wide study of hair colour in UK Biobank explains most of the SNP heritability. Nat. Commun. *9*, 5271.
9. Albertson, R.C., Powder, K.E., Hu, Y., Coyle, K.P., Roberts, R.B., and Parsons, K.J. (2014). Genetic basis of continuous variation in the levels and modular inheritance of pigmentation in cichlid fishes. Mol. Ecol. *23*, 5135–5150.
10. Brien, M.N., Enciso-Romero, J., Lloyd, V.J., Curran, E.V., Parnell, A.J., Morochz, C., Salazar, P.A., Rastas, P., Zinn, T., and Nadeau, N.J. (2022). The genetic basis of structural colour variation in mimetic Heliconius butterflies. Philos. Trans. R. Soc. Lond. B Biol. Sci. *377*, 20200505.
11. Brien, M.N., Enciso-Romero, J., Parnell, A.J., Salazar, P.A., Morochz, C., Chalá, D., Bainbridge, H.E., Zinn, T., Curran, E.V., and Nadeau, N.J. (2019). Phenotypic variation in Heliconius erato crosses shows that iridescent structural colour is sex-linked and controlled by multiple genes. Interface Focus *9*, 20180047.
12. Elkin, J., Martin, A., Courtier-Orgogozo, V., and Santos, M.E. (2022). Meta-analysis of the Genetic Loci of Pigment Pattern Evolution in Vertebrates, . Preprint at. https://doi.org/10.1101/2022.01.01.474697.
13. Figon, F., and Casas, J. (2019). Ommochromes in invertebrates: biochemistry and cell biology. Biol. Rev. *94*, 156–183.
14. Futahashi, R., and Osanai-Futahashi, M. (2021). Pigments in Insects. In Pigments, Pigment Cells and Pigment Patterns, H. Hashimoto, M. Goda, R. Futahashi, R. Kelsh, and T. Akiyama, eds. (Springer). https://doi.org/10.1007/978-981-16-1490-3_1.
15. Spiewak, J.E., Bain, E.J., Liu, J., Kou, K., Sturiale, S.L., Patterson, L.B., Diba, P., Eisen, J.S., Braasch, I., Ganz, J., and Parichy, D.M. (2018). Evolution of Endothelin signaling and diversification of adult pigment pattern in Danio fishes. PLoS Genet. *14*, e1007538.
16. Toomey, M.B., Marques, C.I., Araújo, P.M., Huang, D., Zhong, S., Liu, Y., Schreiner, G.D., Myers, C.A., Pereira, P., Afonso, S., et al. (2022). A mechanism for red coloration in vertebrates. Curr. Biol. *32*, 4201–4214.e12.
17. Twyman, H., Valenzuela, N., Literman, R., Andersson, S., and Mundy, N.I. (2016). Seeing red to being red: conserved genetic mechanism for red cone oil droplets and co-option for red coloration in birds and turtles. Proc. Biol. Sci. *283*, 20161208.
18. Martin, A., and Courtier-Orgogozo, V. (2017). Morphological Evolution Repeatedly Caused by Mutations in Signaling Ligand Genes. In Diversity and Evolution of Butterfly Wing Patterns: An Integrative Approach, T. Sekimura and H.F. Nijhout, eds. (Springer). https://doi.org/10.1007/978-981-10-4956-9_4.
19. Rockman, M.V. (2012). The QTN program and the alleles that matter for evolution: all that's gold does not glitter. Evolution *66*, 1–17.
20. Roulin, A. (2016). Condition-dependence, pleiotropy and the handicap principle of sexual selection in melanin-based colouration. Biol. Rev. Camb. Phil. Soc. *91*, 328–348.
21. Svensson, P.A., and Wong, B.B.M. (2011). Carotenoid-based signals in behavioural ecology: a review. Beyond Behav. *148*, 131–189.
22. Burraco, P., and Orizaola, G. (2022). Ionizing radiation and melanism in Chornobyl tree frogs. Evol. Appl. *15*, 1469–1479.
23. Orr, H.A. (1998). The Population Genetics of Adaptation: The Distribution of Factors Fixed During Adaptive Evolution. Evolution *52*, 935–949.
24. Dembeck, L.M., Huang, W., Magwire, M.M., Lawrence, F., Lyman, R.F., and Mackay, T.F.C. (2015). Genetic Architecture of Abdominal Pigmentation in Drosophila melanogaster. PLoS Genet. *11*, e1005163.
25. Carbone, M.A., Llopart, A., deAngelis, M., Coyne, J.A., and Mackay, T.F.C. (2005). Quantitative Trait Loci Affecting the Difference in Pigmentation Between Drosophila yakuba and D. santomea. Genetics *171*, 211–225.
26. Yeh, S.-D., and True, J.R. (2014). The Genetic Architecture of Coordinately Evolving Male Wing Pigmentation and Courtship Behavior in Drosophila elegans and Drosophila gunungcola. G3 *4*, 2079–2093.

27. Schielzeth, H., Kempenaers, B., Ellegren, H., and Forstmeier, W. (2012). QTL linkage mapping of zebra finch beak color shows an oligogenic control of a sexually selected trait. Evolution *66*, 18–30.

28. Slate, J. (2013). From beavis to beak color: a simulation study to examine how much qtl mapping can reveal about the genetic architecture of quantitative traits. Evolution *67*, 1251–1262.

29. Kardos, M., Husby, A., McFarlane, S.E., Qvarnström, A., and Ellegren, H. (2016). Whole-genome resequencing of extreme phenotypes in collared flycatchers highlights the difficulty of detecting quantitative trait loci in natural populations. Mol. Ecol. Resour. *16*, 727–741.

30. Ju, D., and Mathieson, I. (2021). The evolution of skin pigmentation-associated variation in West Eurasia. Proc. Natl. Acad. Sci. USA *118*, e2009227118.

31. Martin, A.R., Lin, M., Granka, J.M., Myrick, J.W., Liu, X., Sockell, A., Atkinson, E.G., Werely, C.J., Möller, M., Sandhu, M.S., et al. (2017). An Unexpectedly Complex Architecture for Skin Pigmentation in Africans. Cell *171*, 1340–1353.e14.

32. Simcoe, M., Valdes, A., Liu, F., Furlotte, N.A., Evans, D.M., Hemani, G., Ring, S.M., Smith, G.D., Duffy, D.L., Zhu, G., et al. (2021). Genome-wide association study in almost 195,000 individuals identifies 50 previously unidentified genetic loci for eye color. Sci. Adv. *7*, eabd1239.

33. Andrade, P., and Carneiro, M. (2021). Pterin-based pigmentation in animals. Biol. Lett. *17*, 20210221.

34. Vargas-Lowman, A., Armisen, D., Burguez Floriano, C.F., da Rocha Silva Cordeiro, I., Viala, S., Bouchet, M., Bernard, M., Le Bouquin, A., Santos, M.E., Berlioz-Barbier, A., et al. (2019). Cooption of the pteridine biosynthesis pathway underlies the diversification of embryonic colors in water striders. Proc. Natl. Acad. Sci. USA *116*, 19046–19054.

35. Woronik, A., Tunström, K., Perry, M.W., Neethiraj, R., Stefanescu, C., Celorio-Mancera, M.d.l.P., Brattström, O., Hill, J., Lehmann, P., Käkelä, R., and Wheat, C.W. (2019). A transposable element insertion is associated with an alternative life history strategy. Nat. Commun. *10*, 5757.

36. Morehouse, N.I., Vukusic, P., and Rutowski, R. (2007). Pterin pigment granules are responsible for both broadband light scattering and wavelength selective absorption in the wing scales of pierid butterflies. Proc. Biol. Sci. *274*, 359–366.

37. Wijnen, B., Leertouwer, H.L., and Stavenga, D.G. (2007). Colors and pterin pigmentation of pierid butterfly wings. J. Insect Physiol. *53*, 1206–1217.

38. Tunström, K., Woronik, A., Hanly, J.J., Rastas, P., Chichvarkhin, A., Warren, A.D., Kawahara, A.Y., Schoville, S.D., Ficarrotta, V., Porter, A.H., et al. (2023). Evidence for a single, ancient origin of a genus-wide alternative life history strategy. Sci. Adv. *9*, eabq3713.

39. Gerould, J.H. (1943). Genetic and Seasonal Variations of Orange Wing-Color in 'Colias' Butterflies. Proc. Am. Phil. Soc. *86*, 405–438.

40. Ficarrotta, V., Hanly, J.J., Loh, L.S., Francescutti, C.M., Ren, A., Tunström, K., Wheat, C.W., Porter, A.H., Counterman, B.A., and Martin, A. (2022). A genetic switch for male UV iridescence in an incipient species pair of sulphur butterflies. Proc. Natl. Acad. Sci. USA *119*, e2109255118.

41. Silberglied, R.E., and Taylor, O.R. (1973). Ultraviolet Differences between the Sulphur Butterflies, Colias eurytheme and C. philodice, and a Possible Isolating Mechanism. Nature *241*, 406–408.

42. Grula, J.W., and Taylor, O.R. (1980). Some Characteristics of Hybrids Derived from the Sulfur Butterflies, Colias eurytheme and C. philodice: Phenotypic Effects of the X-Chromosome. Evolution *34*, 673–687.

43. Grula, J.W., McChesney, J.D., and Taylor, O.R. (1980). Aphrodisiac pheromones of the sulfur butterfliesColias eurytheme andC. Philodice (Lepidoptera, Pieridae). J. Chem. Ecol. *6*, 241–256.

44. Grula, J.W., and Taylor, O.R. (1979). The inheritance of pheromone production in the sulphur butterflies Colias eurytheme and C. Philodice. Heredity *42*, 359–371.

45. Grula, J.W., and Taylor, O.R. (1980). The effect of X-chromosome inheritance on mate-selection behavior in the sulfur butterflies, Colias eurytheme and C. philodice. Evolution *34*, 688–695.

46. Presgraves, D.C. (2018). Evaluating genomic signatures of "the large X-effect" during complex speciation. Mol. Ecol. *27*, 3822–3830.

47. Wang, B., and Porter, A.H. (2004). An AFLP-Based Interspecific Linkage Map of Sympatric, Hybridizing Colias Butterflies. Genetics *168*, 215–225.

48. Weller, H.I., and Westneat, M.W. (2019). Quantitative color profiling of digital images with earth mover's distance using the R package colordistance. PeerJ *7*, e6398.

49. Hovanitz, W. (1944). The Ecological Significance of the Color Phases of Colias Chrysotheme in North America. Ecology *25*, 45–60.

50. Cockerham, C.C. (1986). Modifications in Estimating the Number of Genes for a Quantitative Character. Genetics *114*, 659–664.

51. Otto, S.P., and Jones, C.D. (2000). Detecting the undetected: estimating the total number of loci underlying a quantitative trait. Genetics *156*, 2093–2107.

52. Broman, K.W., Wu, H., Sen, S., and Churchill, G.A. (2003). R/qtl: QTL mapping in experimental crosses. Bioinforma. Oxf. Engl. *19*, 889–890.

53. Francescutti, C.M., Martin, A., and Hanly, J.J. (2022). Knockdowns of red Malphigian tubules reveal pigmentation roles in the milkweed bug. J. Exp. Zool. B Mol. Dev. Evol. *338*, 382–387.

54. Grant, P., Maga, T., Loshakov, A., Singhal, R., Wali, A., Nwankwo, J., Baron, K., and Johnson, D. (2016). An Eye on Trafficking Genes: Identification of Four Eye Color Mutations in Drosophila. G3 *6*, 3185–3196.

55. Silberglied, R.E., and Taylor, O.R. (1978). Ultraviolet reflection and its behavioral role in the courtship of the sulfur butterflies Colias eurytheme and C. philodice (Lepidoptera, Pieridae). Behav. Ecol. Sociobiol. *3*, 203–243.

56. Wilts, B.D., Wijnen, B., Leertouwer, H.L., Steiner, U., and Stavenga, D.G. (2017). Extreme Refractive Index Wing Scale Beads Containing Dense Pterin Pigments Cause the Bright Colors of Pierid Butterflies. Adv. Opt. Mater. *5*, 1600879.

57. Figon, F., Hurbain, I., Heiligenstein, X., Trépout, S., Lanoue, A., Medjoubi, K., Somogyi, A., Delevoye, C., Raposo, G., and Casas, J. (2021). Catabolism of lysosome-related organelles in color-changing spiders supports intracellular turnover of pigments. Proc. Natl. Acad. Sci. USA *118*, e2103020118.

58. Ghiradella, H. (2010). Chapter 4 - Insect Cuticular Surface Modifications: Scales and Other Structural Formations. In Advances in Insect Physiology, J. Casas and S.J. Simpson, eds. (Academic Press), pp. 38.135–180.

59. Fenner, J., Ficarrotta, V., Colombara, A., Smith, H., Evans, K., Range, R., and Counterman, B.A. (2022). Seasonal polyphenism of wing colors and its influence on sulphur butterfly diversification. Preprint at bioRxiv. https://doi.org/10.1101/2022.08.10.503521.

60. De Castro, S., Peronnet, F., Gilles, J.-F., Mouchel-Vielh, E., and Gibert, J.-M. (2018). bric à brac (bab), a central player in the gene regulatory network that mediates thermal plasticity of pigmentation in Drosophila melanogaster. PLoS Genet. *14*, e1007573.

61. Kopp, A., Graze, R.M., Xu, S., Carroll, S.B., and Nuzhdin, S.V. (2003). Quantitative trait loci responsible for variation in sexually dimorphic traits in Drosophila melanogaster. Genetics *163*, 771–787.

62. Rogers, W.A., Salomone, J.R., Tacy, D.J., Camino, E.M., Davis, K.A., Rebeiz, M., and Williams, T.M. (2013). Recurrent Modification of a Conserved Cis-Regulatory Element Underlies Fruit Fly Pigmentation Diversity. PLoS Genet. *9*, e1003740.

63. Porter, A.H., and Levin, E.J. (2007). Parallel evolution in sympatric, hybridizing species: performance of Colias butterflies on their introduced host plants. Entomol. Exp. Appl. *124*, 77–99.

64. Nokelainen, O., Galarza, J.A., Kirvesoja, J., Suisto, K., and Mappes, J. (2022). Genetic colour variation visible for predators and conspecifics is concealed from humans in a polymorphic moth. J. Evol. Biol. *35*, 467–478.

65. Boyle, E.A., Li, Y.I., and Pritchard, J.K. (2017). An expanded view of complex traits: from polygenic to omnigenic. Cell *169*, 1177–1186.
66. Yong, L., Peichel, C.L., and McKinnon, J.S. (2015). Genetic Architecture of Conspicuous Red Ornaments in Female Threespine Stickleback. G3 *6*, 579–588.
67. Xu, S. (2003). Theoretical Basis of the Beavis Effect. Genetics *165*, 2259–2268.
68. Mackay, T.F.C., Stone, E.A., and Ayroles, J.F. (2009). The genetics of quantitative traits: challenges and prospects. Nat. Rev. Genet. *10*, 565–577.
69. Hoffmann, R.J. (1974). Environmental control of seasonal variation in the butterfly Colias eurytheme: Effects of photoperiod and temperature on pteridine pigmentation. J. Insect Physiol. *20*, 1913–1924.
70. Remington, C.L. (1954). The genetics of Colias (Lepidoptera). Adv. Genet. *6*, 403–450.
71. Jacobs, M.D., and Watt, W.B. (1994). Seasonal Adaptation vs Physiological constraint: Photoperiod, Thermoregulation and Flight in Colias Butterflies. Funct. Ecol. *8*, 366–376.
72. Kingsolver, J.G. (1995). Fitness consequencs of seasonal polyphenism in western white butterflies. Evolution *49*, 942–954.
73. Kingsolver, J.G., and Wiernasz, D.C. (1991). Seasonal Polyphenism in Wing-Melanin Pattern and Thermoregulatory Adaptation in Pieris Butterflies. Am. Nat. *137*, 816–830.
74. Beldade, P., Mateus, A.R.A., and Keller, R.A. (2011). Evolution and molecular mechanisms of adaptive developmental plasticity. Mol. Ecol. *20*, 1347–1363.
75. Lafuente, E., and Beldade, P. (2019). Genomics of Developmental Plasticity in Animals. Front. Genet. *10*, 720.
76. Oster, I. (1954). New mutants. red: Red Malpighian tubules. Drosoph. Inf. Serv. *28*, 77.
77. Henikoff, S. (1979). Position Effects and Variegation Enhancers in an Autosomal Region of Drosophila melanogaster. Genetics *93*, 105–115.
78. Breen, T.R., and Harte, P.J. (1991). Molecular characterization of the trithorax gene, a positive regulator of homeotic gene expression in Drosophila. Mech. Dev. *35*, 113–127.
79. Figon, F., Deravi, L.F., and Casas, J. (2021). Barriers and Promises of the Developing Pigment Organelle Field. Integr. Comp. Biol. *61*, 1481–1489.
80. Aslaksen, E., and Hadorn, E. (1957). Untersuchungen über eine Mutante (red) von Drosophila melanogaster mit roten Malpighischen Gefässen. Arch Julius Klaus-Stift Vererbungsforsch Sozialanthropol U Rassenhyg *32*, 464–469.
81. Ferré, J., Silva, F.J., Real, M.D., and Ménsua, J.L. (1986). Pigment patterns in mutants affecting the biosynthesis of pteridines and xanthommatin in Drosophila melanogaster. Biochem. Genet. *24*, 545–569.
82. Wessing, A., and Bonse, A. (1966). Natur und Bildung des roten Farbstoffes in den Nierentubuli der Mutante "red" von Drosophila melanogaster. Z. Naturforsch. B Chem. Sci. *21*, 1219–1223.
83. Shoup, J.R. (1966). The development of pigment granules in the eyes of wild type and mutant Drosophila melanogaster. J. Cell Biol. *29*, 223–249.
84. Tearle, R. (1991). Tissue specific effects of ommochrome pathway mutations in Drosophila melanogaster. Genet. Res. *57*, 257–266.
85. Allan, A.K., Du, J., Davies, S.A., and Dow, J.A.T. (2005). Genome-wide survey of V-ATPase genes in Drosophila reveals a conserved renal phenotype for lethal alleles. Physiol. Genom. *22*, 128–138.
86. Sun-Wada, G.-H., Wada, Y., and Futai, M. (2003). Lysosome and lysosome-related organelles responsible for specialized functions in higher organisms, with special emphasis on vacuolar-type proton ATPase. Cell Struct. Funct. *28*, 455–463.
87. Yan, Y., Denef, N., and Schüpbach, T. (2009). The vacuolar proton pump, V-ATPase, is required for notch signaling and endosomal trafficking in Drosophila. Dev. Cell *17*, 387–402.
88. Merkulova, M., Păunescu, T.G., Azroyan, A., Marshansky, V., Breton, S., and Brown, D. (2015). Mapping the H+ (V)-ATPase interactome: identification of proteins involved in trafficking, folding, assembly and phosphorylation. Sci. Rep. *5*, 14827.
89. Castroflorio, E., den Hoed, J., Svistunova, D., Finelli, M.J., Cebrian-Serrano, A., Corrochano, S., Bassett, A.R., Davies, B., and Oliver, P.L. (2021). The Ncoa7 locus regulates V-ATPase formation and function, neurodevelopment and behaviour. Cell. Mol. Life Sci. *78*, 3503–3524.
90. Eaton, A.F., Brown, D., and Merkulova, M. (2021). The evolutionary conserved TLDc domain defines a new class of (H+)V-ATPase interacting proteins. Sci. Rep. *11*, 22654.
91. Tan, Y.Z., Abbas, Y.M., Wu, J.Z., Wu, D., Keon, K.A., Hesketh, G.G., Bueler, S.A., Gingras, A.C., Robinson, C.V., Grinstein, S., and Rubinstein, J.L. (2022). CryoEM of endogenous mammalian V-ATPase interacting with the TLDc protein mEAK-7. Life Sci. Alliance *5*, e202201527.
92. Saenko, S.V., Teyssier, J., van der Marel, D., and Milinkovitch, M.C. (2013). Precise colocalization of interacting structural and pigmentary elements generates extensive color pattern variation in Phelsumalizards. BMC Biol. *11*, 105.
93. Ramos-Balderas, J.L., Carrillo-Rosas, S., Guzman, A., Navarro, R.E., and Maldonado, E. (2013). The zebrafish mutants for the V-ATPase subunits d, ac45, E, H and c and their variable pigment dilution phenotype. BMC Res. Notes *6*, 39.
94. Wakamatsu, K., Zippin, J.H., and Ito, S. (2021). Chemical and biochemical control of skin pigmentation with special emphasis on mixed melanogenesis. Pigment Cell Melanoma Res. *34*, 730–747.
95. Fraïsse, C., and Sachdeva, H. (2021). The rates of introgression and barriers to genetic exchange between hybridizing species: sex chromosomes vs autosomes. Genetics *217*, iyaa025.
96. Wilson Sayres, M.A. (2018). Genetic Diversity on the Sex Chromosomes. Genome Biol. Evol. *10*, 1064–1078.
97. Butlin, R.K., and Smadja, C.M. (2018). Coupling, Reinforcement, and Speciation. Am. Nat. *191*, 155–172.
98. Unbehend, M., Kozak, G.M., Koutroumpa, F., Coates, B.S., Dekker, T., Groot, A.T., Heckel, D.G., and Dopman, E.B. (2021). bric à brac controls sex pheromone choice by male European corn borer moths. Nat. Commun. *12*, 2818.
99. Estalles, C., Turbek, S.P., José Rodríguez-Cajarville, M., Silveira, L.F., Wakamatsu, K., Ito, S., Lovette, I.J., Tubaro, P.L., Lijtmaer, D.A., and Campagna, L. (2022). Concerted variation in melanogenesis genes underlies emergent patterning of plumage in capuchino seedeaters. Proc. Biol. Sci. *289*, 20212277.
100. Wang, B. (2005). Introgression and genomic differentiation in sympatric, hybridizing Colias butterflies. Dr. Diss.. *Available Proquest* 1–149.
101. MacLachlan, G., Hurlburt, J., Suarez, M., Wong, K.L., Burke, W., Lewis, T., Gallo, A., Flidr, J., Gabiam, R., Nicholas, J., et al. (2020). Building a shared resource HPC Center across University Schools and Institutes: A case study. Preprint at arXiv. https://doi.org/10.48550/arXiv.2003.13629.
102. Ren, A., Day, C.R., Hanly, J.J., Counterman, B.A., Morehouse, N.I., and Martin, A. (2020). Convergent Evolution of Broadband Reflectors Underlies Metallic Coloration in Butterflies. Front. Ecol. Evol. *8*.
103. Chavent, M., Kuentz-Simonet, V., Liquet, B., and Saracco, J. (2012). ClustOfVar: An R Package for the Clustering of Variables. J. Stat. Software *50*, 1–16.

STAR★METHODS

KEY RESOURCES TABLE

REAGENT or RESOURCE	SOURCE	IDENTIFIER
Critical commercial assays		
DNeasy Blood and Tissue Kit (50)	Qiagen	69504
Taq 2x Master Mix	New England Biolabs	M0270
Plastic Pestle and 1.5mL Tube	Bel-Art	F19923-0000
Cas9-2xNLS protein	QB3 Macrolab, UC Berkeley	N/A
Phenol Red, 0.5%	Sigma-Aldrich	P0290-100ML
Low EDTA Tris buffer, pH 8.0	Quality Biological	351-324-721
Deposited data		
Colias eurytheme reference genome assembly	Tunström et al.[38]	ENA:PRJEB43860
Colias eurytheme x philodice, resequencing of wild-caught individual from an admixed population (MD, USA)	Ficarrotta et al.[40]	NCBI:PRJNA663300; Table S1A in https://doi.org/10.1073/pnas.2109255118
Colias eurytheme x philodice, resequencing of individuals from backcross and F2 mapping broods	Ficarrotta et al.[40]	NCBI:PRJNA719421; Table S1D in https://doi.org/10.1073/pnas.2109255118
High-resolution wing scans of all butterfly specimens	This paper	https://doi.org/10.5061/dryad.5dv41ns9t
Experimental models: Organisms/strains		
Colias eurytheme, wild-caught	Alfalfa fields in Hampshire Co. (MA, 2000–2001) and in Frederick Co. (MD, 2020-21)	NCBI:txid42296
Colias philodice, wild-caught	Alfalfa fields in Hampshire Co. (MA, 2000–2022) and in Frederick Co. (MD, 2020-21)	NCBI:txid72851
Colias eurytheme x philodice F1 and F2 broods	Wang PhD dissertation, 2005	ISBN: 978-0-542-19832-8
Colias eurytheme, bab G0 crispants	Ficarrotta et al.[40]	Figure S11; https://doi.org/10.1073/pnas.2109255118
Oligonucleotides		
sgRNA targeting sequence, *Ceu_red_exon1: 5′-GTTTACGTCAAACATGGAGG*	Synthego	N/A
sgRNA targeting sequence, *Ceu_bab_sgRNA1: 5′-ACTGTTGGGGCGAGCCGGG*	Synthego	SI Appendix; https://doi.org/10.1073/pnas.2109255118
sgRNA targeting sequence, *Ceu_bab_sgRNA2: 5′-CGGCGGGCCCGGCTCCTCG*	Synthego	SI Appendix; https://doi.org/10.1073/pnas.2109255118
Software and algorithms		
Geneious R10	Geneious	N/A
R/colordistance package v.1.1.2	GitHub/Hannah Weller	URL: http://hiweller.github.io
R/ClustOfVar	GitHub/Marie Chavent	URL: http://github.com/cran/ClustOfVar
R/qtl	GitHub/Karl Broman	URL: https://github.com/kbroman/qtl
Custom code used for QTL analysis	This paper	https://doi.org/10.5061/dryad.5dv41ns9t
Other		
Full-Size Seedling Light Cart – 16 Trays, 512 Watts	Johnny's Selected Seeds	7295
32-watt T8 Gro-Lux wide-spectrum grow tubes	Sylvania Lighting	22362
Organic Lana Vetch (*Vicia villosa*)	Hearne Seeds	N/A

(*Continued on next page*)

Continued

REAGENT or RESOURCE	SOURCE	IDENTIFIER
Plant Germination Drip Trays - 10" × 10″ with no drain holes	Amazon/Handy Pantry	B08379JNCS
Plant Germination Growing Trays - 10" × 10″ with drain holes	Amazon/Handy Pantry	B00UT72M5U
Plant Germination Drip Trays - 10" × 20″ with no drain holes	Amazon/Handy Pantry	B08377BPCJ
Plant Germination Growing Trays - 10" × 20″ with drain holes	Amazon/Handy Pantry	B0837742LG
Hemp Matting roll 10″ × 120"	Terrafibre	GMR-10120-1
Butterfly habitat pop-up cage, 15.7″ × 15.7" x 23.6"	Amazon/Restcloud	B074ZHXF48
Benzalkonium Chloride solution, 50%	Sigma-Aldrich	63249-500ML
Small Clear Plastic Souffle/Cup Lid	Solo	PL100N
Borosilicate capillaries with filament	WorldPrecision Instruments	18100F-3
Gravity needle puller	Narishige International	PC-10
Three-axis MM33 right-handed manipulator	Drummond Scientific	3-000-024-R
Single pressure micro-injectors with footswitch	Tritech Research Inc.	MINJ-1
Pulse-length control module	Tritech Research Inc.	MINJ-2
Needle holder	Tritech Research Inc.	MINJ-4
Compressed air faucet adapter	Tritech Research Inc.	MINJ-38NPT14QC
Polyurethane tubing 1/4″ OD, 1/8″ ID	Tritech Research Inc.	TT-1-4OD
3-way and 4way Tee air splitters	Tritech Research Inc.	MINJ-3TQC; MINJ4TQC
Brass compression fittings	Tritech Research Inc.	MINJ-5
Compression fittings	Tritech Research Inc.	MINJ-6
Binocular stereomicroscopes with 10–25× magnification	Any	N/A
Cardboard Freezer Box, with 196 place PCR inserts	Argos Technologies	FBZ-1196W

RESOURCE AVAILABILITY

Lead contact

Further information and requests for resources, protocols and reagents should be directed to and will be fulfilled by lead contact, Joseph Hanly (joe.hanly@gmail.com).

Materials availability

This study did not generate new unique reagents.

Data and code availability

- All experimental model organisms/strains are listed in the key resources table. All images and measurements have been deposited at Dryad, and are publicly available. DOIs are listed in the key resources table.
- All code used for statistical analysis and figure plotting has been deposited at Dryad and is publicly available. DOIs are listed in the key resources table.
- Any additional information required to reanalyze the data reported in this paper is available from the lead contact upon request.
- The color phenotypes in this article involve nuanced gradations of yellow and orange that may be difficult to perceive for people who are color vision deficient. Hue-shifted versions of all main figures are accessible online for dichromat readers as supplementary material.

EXPERIMENTAL MODEL AND STUDY PARTICIPANT DETAILS

Butterfly mapping broods

Interspecies F_1, F_2 and backcrosses between *C. eurytheme* and *C. philodice* were generated in 2000–2001 from wild individuals caught in and around Amherst, MA, as previously described.[47,100] A former publication describes DNA extraction procedures and 2b-RADseq linkage maps for one F_2 brood and two backcross broods.[38,40] All broods were reared under summer conditions (27°C and LD 14:10 h) on fresh alfalfa cuttings placed in large Petri dishes in two growth chambers. Dishes were moved within and among growth chambers at 3-day intervals to randomise environmental growth chamber effects. Adults were stored in labelled glassine envelopes at −80°C shortly after emergence until thorax tissue sampling for DNA extraction in 2018.

Butterfly mosaic KOs

For CRISPR mutagenesis, *C. eurytheme* gravid females were wild-caught on organic alfalfa fields in Buckeystown, MD (kind permission of Dr. Scott Barrao, Hedgeapple Farms) before being brought in the lab for oviposition on alfalfa cuttings (Ficarrotta et al. 2022). Larvae were reared on hydroponic trays of 7–21 d old vetch sprouts contained in large collapsible cages, in a temperature controlled greenhouse maintained at 27°C–29°C and with an automated misting system, in August-September 2020 (*bab* KOs) and June-September 2021 (*red* KOs). Total developmental time at 27°C–29°C is about 26 d, with an average egg hatching time of 70 h AEL, and an adult emergence time of 132 h after pupa formation. Emerged adults were pinned or their wings stored in glassine envelopes for further imaging.

Larval host plants

Alfalfa plants (*Medicago sativa*) were grown as mature plants in pots containing a soil mix with vermiculite. Fresh plant cuttings with young leaves were used for larval rearing, or placed in a water cup for oviposition. Dry seeds of Lana hairy vetch (*Vicia villosa* var. Lana) were weighed, soaked overnight in water for rehydration, spread on water-saturated hemp fiber mats placed in hydroponic trays at a density of 7.5 g/in^2 (dry weight), germinated in the dark for 72 h with occasional misting with water, fertilised with a 200 ppm N solution (1 g/L of NPK 20:20:20 fertiliser), and sprouted on a seedling light cart equipped with 32 W T8 wide-spectrum tubes for 72 h before removal from the grow lights. Hydroponic trays were occasionally bottom-watered with a 50 ppm N solution and provided to larvae for feeding within 14 d after germination.

METHOD DETAILS

Color imaging

For QTL mapping, we scanned the dorsal and ventral surface of forewings and hindwings from the three previously described broods, plus wings from four additional broods, with an Epson Perfection V600 scanner with a 24-colour correction card and greyscale standards. All images are deposited on Dryad.

For color quantification in *red* CRISPR experiments, dorsal wing regions of interest situated between the M_1-Cu_2 veins were digitised with a Keyence VHX-5000 microscope, and VH-Z100T zoom lens under constant lighting conditions (including a covering of the microscope to prevent environmental light variation), and using stitch scans of >70 images at the 200× magnification. Images of 1000 x 1000 pixels were then isolated from areas with no damage, including mutant and adjacent wild-type clones from crispant individuals.

All imaging was conducted with constant lighting conditions and acquisition parameters. Whole specimens were imaged using the VH-Z00R lens at a lens magnification set-up of 50x, or a Nikon D5300 camera mounted with a Micro-Nikkor 105mm f/2.8G lens using an f/16 aperture and diffused LED illumination. Microphotographs of wing details were imaged using the VH-Z100T lens at magnification set-ups of 200×, 500×, and 700×. Microphotographs of single scales were acquired using a Nikon D5300 camera mounted on an a Varimag II camera adapter at a 2× magnification setting, a trinocular AmScope ME580-2L metallurgical microscope with a polarizer and analyzer, and a BoliOptics LMPlan Achromatic 50×/NA 0.6 objective.

CRISPR mutagenesis

Cas9-2xNLS recombinant protein stock was dispatched in 2.5 μL aliquots after dilution to a concentration of 1000 ng/μL in 2x injection buffer (7.4 pH, 1 mM NaH_2PO_4, 1 mM Na_2HPO_4, 10 mM KCl). Synthetic sgRNAs were dispatched at 500 ng/μL in 2.5 μL aliquots after dilution in Low EDTA Tris buffer (pH 8.0, 10mM Tris-HCl, 0.1 mM EDTA). Aliquots were stored at −80°C and mixed prior to injection. Eggs were collected from *C. eurytheme* wild-caught gravid females, surface-decontaminated with 5% Benzalkonium Chloride for 1–2 min, rinsed with distilled water, air-dried and placed upright on double-sided tape rendered less sticky with paper towel fibers. Syncytial embryos up to 4 h AEL were micro-injected with a 250:125 ng/μL (for *red*) or 500:250 ng/μL (for *bab*) Cas9:sgRNA mix using pulled borosilicate capillaries. Injection dishes were moved to a plastic container humidity-saturated with a wet paper towel for 48 h to avoid desiccation before proper egg healing, and then placed face down on 7–14 d old vetch trays for hatching. All the *bab* crispants characterised in this study were generated in a previous publication.[40]

UV macrophotography and microphotography

All imaging in the UV-A range was performed using a full-spectrum converted Lumix G3 camera mounted under the illumination of two CFL BlackLight 13 Watt T3 Spiral Light Bulbs (General Electric, USA). All lens set-ups were mounted with a U-Venus-Filter (Baader Planetarium, Germany), which blocks visible light above 400 nm. For imaging of whole specimens, an EL-Nikkor 50 mm f/2.8 N lens was mounted with about 60 mm of extension using focusing helicoids, while for magnified views of wing details, that same lens was reverse-mounted and provided additional extension using a sliding bellows.

Scanning Electron Microscopy

Scales of interest were placed on carbon tape and sputter coated with a 10–12 nm layer of gold.[102] SEM images were acquired on a FEI Teneo LV SEM, using the Everhart-Thornley detector and beam parameters of 2.00 kV/25 pA with a 10 μs dwell time. Scale cryofracturing was performed as previously described.[40,102]

Image post-processing

No post-processing was performed on the image datasets acquired with the Epson scanner and Keyence microscopes, i.e., the images used for color profile analyses. In order to correct for slight overexposure in all visible (Nikon D5300) and UV-A (Lumix G3) images of whole pinned specimens, an overexposure compensation (Black Point value of +30 and White Point value of −15) was applied in post-processing using the Levels function in Adobe Photoshop. This adjustment uniformly changes luminosity and does not affect hues visibly.

QUANTIFICATION AND STATISTICAL ANALYSIS

Automated color scoring

Images were processed with the *R* package *colordistance*.[48] Cropped images of each wing and wing surface were imported, and the CIELAB value determined for 10,000 randomly sampled pixels per image. Using the function *getLabHist*, thresholds were applied to remove the white background and brown-black pixels. The remaining pixels within retained *L*a*b** (Lab) value ranges were placed into 50 bins of the *b** component (with no subdivisions of *L** or *a**), with lower values corresponding to 'oranger' wings and high values corresponding to 'yellower' wings. This allowed a distribution of pixel hues to be rapidly and repeatedly determined from thousands of images. We took the number of the bin containing the highest number of pixels (the 'max bin') value as the phenotypic score for each individual and used this value for QTL analysis. Because this score does not directly correspond to one axis of Lab parameter space, we named it the 'yellow score' to reduce ambiguity.

Landmarking, morphometrics and clustering analysis

Individual measurements were taken using FIJI (Figures S7A and S7B). Sizes were calibrated with a ruler included in the wing scans. Where possible, pattern elements were measured from left and right wings to ensure consistency of measurements; likewise, size measurements were taken from both the dorsal and ventral wing surfaces. Principal component analysis of wing measurements was performed using the base-R function prcomp(), and plotted with density curves with ggplot2.

Many of the measured variables may be strongly related to each other and therefore contain the same information. In order to identify groups of independent variables we clustered the traits using the R package *ClustOfVar*.[103] Briefly, data was log-transformed and a trait hierarchy constructed (Figure S7D), and the dispersion of the Rand index for clusters was observed to support the selection of 5 clusters. A latent variable per cluster was then calculated for every individual, and these latent variables were used for the QTL analyses (Figure S8).

QTL analysis and gene identification

For linkage mapping and QTL analysis, we used the published linkage maps for one F_2 and two BC broods, which we previously used for genome assembly and mapping of UV iridescent color (Ficarrotta et al. 2022). For each variable (yellow score and the five cluster latent variables), we performed single QTL genome scans in *R/qtl*[52] with Haley-Knott regression, calculating significance thresholds for each scan with 1,000 permutations, and defined 95% Bayes credible intervals for each significant peak.

Two-QTL genome scans were also run with Haley-Knott regression and 500 permutations. The goodness of fit of each significant two-QTL model was examined with the function fitqtl(), which provided the percentage of variance explained by the interaction. We further examined multiple-QTL models, assessing the probability that additional loci might explain a significant fraction of variation when accounting for the detected intervals, though no additional significant QTL were detected this way.

Colour-enhanced figures

The main figures of this manuscript are presented as Figures S9–S15 with enhanced hues that are more readily perceived by readers with the most common color vision deficiencies. Pixels with Hue values 35°–60° (Figures 1 and 2), or 30°–60° (Figures 4–6), i.e., the range of orange-yellow pixels observed in the included wing images, were rotated −180° in HSV space using Adobe Photoshop. For figures presenting QTL plots (Figures 3 and 7), Red Channels in RGB space were transposed into the Blue Channel to create heatmaps with a magenta-green color scale using Adobe Photoshop.